The *in vivo* effect of integrin α11-deficiency and PDGFR inhibition in breast cancer

By
Tore-Andre Brodahl

This thesis is submitted in partial fulfilment of the requirements for the degree of Master of Science

Department of Biomedicine
Faculty of Medicine
University of Bergen, Norway

October 2018

Acknowledgements

This master thesis is based on work carried out at the Department of Biomedicine, University of Bergen, in the period from December 2017 to October 2018.

First and foremost I would like to thank my supervisor, Professor Linda Stuhr for her support and guidance throughout this thesis. You always found time for all my questions and when I needed guidance. Your joy and enthusiasm are much appreciated.

I would also like to express my gratitude to PhD candidate Hilde Ytre-Hauge Smeland for her assistance in the laboratory and in the writing process. Further, I would like to thank Gerd Signe Salvesen for all her help and technical assistance in the laboratory and at the animal facility.

Last, but not least I would like to thank my family for their love and support during this master thesis. I would like to thank my parents for their patience and many hours spent babysitting. I would especially like to express my gratitude to my wife and daughter, you are the joy of my life.

Bergen, 2018

Tore-Andre Brodahl

Abstract

Background: The tumor microenvironment is a major contributor to breast cancer progression. The abnormal composition of the extracellular matrix and its deregulated interactions with stromal cells, which is characterizing features in breast cancer, promotes tumor progression and poses an obstacle cancer therapy through increased interstitial fluid pressure. The aim of this study was to evaluate the effect of stromal integrin α11-deficiency and PDGFR-inhibition on tumor growth, interstitial fluid pressure, angiogenesis, and collagen density using the murine E0771 triple-negative breast cancer model.

Methods: SCID mice with and without integrin α11-deficiency were injected with the murine E0771 cell line into the mammary fat pad. The mice were randomly divided into four groups, where two groups received treatment with the PDGFR-inhibitor Gleevec (100 mg/kg) by gavage once a day over a four-day period. The two remaining groups received water by gavage. The tumor growth was measured by caliper, the interstitial fluid pressure was measured with the wick-in-needle technique, microvessel density by immunohistochemical anti-CD31 staining, and the collagen density by picrosirius red staining.

Results: Integrin α11-deficiency significantly reduced the interstitial fluid pressure, microvessel density, and collagen density. Gleevec significantly reduced the interstitial fluid pressure, and microvessel density. No effects were seen on tumor growth by either integrin α11-deficiency, or PDGFR-inhibition by Gleevec. No synergistic or additive effect was observed in response to inhibition of PDGF/PDGFR signalling in the α11-deficient groups.

Conclusion: This study show the importance of integrin α11β1 in the regulation of the interstitial fluid pressure, angiogenesis and collagen density in the murine E0771 triple-negative breast cancer model. All these features are critical features in tumor progression, thus indicating that integrin α11 may represent an attractive therapeutic target in adjuvant settings. Gleevec was found to significantly reduce the interstitial fluid pressure, and the microvessel density. Suggesting that PDGF/PDGFR signalling is important in the regulation of pressure homeostasis and angiogenesis.

Table of contents

Selected abbreviations

A	Capillary surface area
ABC	Avidin-biotin complex
COP_{cap}	Capillary colloid osmotic pressure
COP_{if}	Interstitial colloid osmotic pressure
ECM	Extracellular matrix
EGF	Epidermal growth factor
ER	Estrogen receptor
FGF	Fibroblast growth factor
HER2	Human epidermal growth factor receptor 2
IFP	Interstitial fluid pressure
IHC	Immunohistochemistry
IMD	Integrin-mediated death
J_v	Volume flux of fluid
KO	Knock-out
L_p	Hydraulic conduction
LOX	Lysyl oxidase
MMP	Matrix metalloproteinase
MVD	Microvessel density
P_{cap}	Capillary hydrostatic pressure
P_{if}	Interstitial hydrostatic pressure
PDGF	Platelet-derived growth factor
PDGFR	Platelet-derived growth factor receptor
PgR	Progesterone receptor
PI	Propidium iodine
S	Surface area available for filtration
SCID	Severe combined immune deficient
SEM	Standard error of mean
TGF	Transforming growth factor
TNBC	Triple-negative breast cancer
TNF	Tumor necrosis factor
VEGF	Vascular endothelial growth factor
WIN	Wick-in-needle
WT	Wild type
σ	Osmotic reflection coefficient

1 Introduction

1.1 Cancer

Cancer is one of the leading causes of death worldwide (Ferlay et al., 2015). In 2012, approximately 8.2 million died from cancer, and 14.1 million new cases of cancer were reported. By 2030, cancer is predicted to cause 13.2 million deaths and 20.3 million new incidents (Bray et al., 2012). In Norway, a total of 32 592 new cases of cancer were reported in 2015 (Kreftregisteret.no, 2016).

Cancer is a group of genetic diseases, characterized by unregulated cell growth and the ability to spread from its site of origin to other sites in the body (metastasize) (Pecorino, 2012). Over 100 different types of cancer have been classified, separated by distinguishing characteristics from the tissue of origin. Cancers can grow as solid tumors or as liquid tumors (e.g. leukemias). A tumor is usually defined as either benign (non-invasive) or malignant (invasive).

Cancer is caused by genetic and epigenetic alterations that facilitate mutational activation of oncogenes and inactivation of tumor-suppressor genes (Vogelstein et al., 2013; Vogelstein and Kinzler, 2015). Mutations in these genes, called “driver-gene” mutations, directly promote tumorigenesis by conferring a selective growth advantage to the tumor cell (Vogelstein and Kinzler, 2004). Accumulation of driver-gene mutations enable tumors to evolve from a breakthrough phase, where a single cell proliferates abnormally, to an expansion phase where the growing tumor thrives in its local environment (Vogelstein and Kinzler, 2015). The last phase is the invasive phase, where subsequent driver-gene mutations enable the tumor to invade surrounding and distant tissue.

Cancer evolves in a progressive manner, gradually acquiring properties necessary for malignant development (Vogelstein et al., 2013). The defining cellular traits of cancer development have been classified into ten distinct “hallmarks” by Hanahan and

Weinberg (Figure 1.1) (Hanahan and Weinberg, 2000, 2011). The hallmarks of cancer include enabling traits such as genomic instability and mutation, tumor-promoting inflammation, deregulation of cellular energetics and avoidance of immune destruction. In addition, a growing tumor need to develop sustained proliferative signalling and obtain replicative immortality, evade growth suppressors and apoptosis, induce angiogenesis and activate invasion and metastasis.

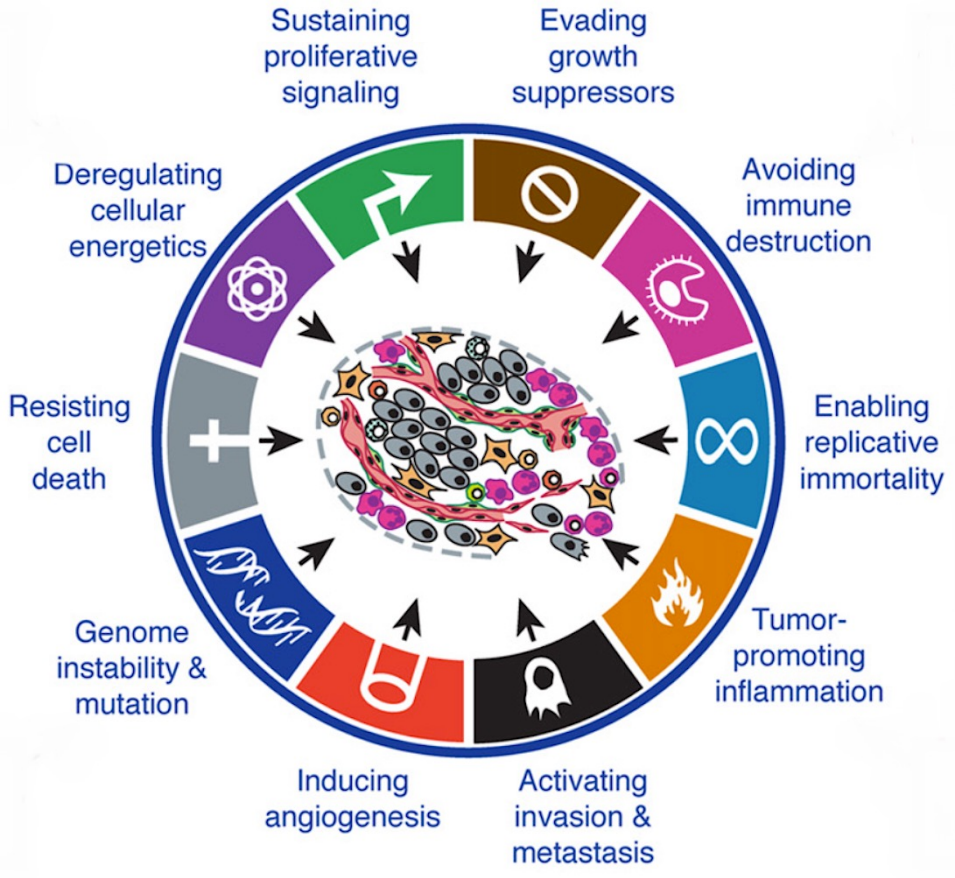

Figure 1.1: The hallmarks of cancer

The Hallmarks of cancer are ten characterizing traits of cancer proposed by Hanahan and Weinberg. These hallmarks are gradually acquired during the progressive development of cancer. Figure from (Hanahan and Weinberg, 2011) with permission.

1.2 Breast cancer

Breast cancer is the most common type of cancer in women worldwide, with 1.67 million incidents in 2012 (Ferlay et al., 2015). This translates to 25% out of all cancer incidents in women. In Norway, 3371 new cases of breast cancer were diagnosed in 2015 (Kreftregisteret.no, 2016). Upon diagnosis, a breast tumor can be confined to the primary lesion (*in situ*); occupy the structures beneath the epithelial basement membrane (*invasive*); or have disseminated beyond the breast parenchyma to the regional lymph nodes, bone, brain, liver or lungs through lymphatic and blood vessels (*metastatic*) (Schito and Rey, 2017).

Breast cancer is now recognized as a diverse set of diseases characterized by heterogeneity in histology, genomic aberrations and protein expression that influence treatment response and patient outcome (Whittle et al., 2015). Histologically, breast cancer is usually classified based on the site from which the tumor originated (Makki, 2015). The most common morphological subtype of breast cancer is Invasive Carcinoma of No Special Type (IC-NST), previously called Invasive Ductal Carcinoma (IDC), which originate from the inner lining epithelium of the milk ducts (Figure 1.2)(Makki, 2015; Lal et al., 2017). Invasive ductal carcinoma accounts for approximately 80% of breast cancers. The second most common morphological subtype, accounting for approximately 10% of breast cancers, is Invasive Lobular Carcinoma (ILC), which originates from the lobules that supply the ducts with milk. Other less common subtypes include medullary, metaplastic, tubular and mucinous, all of which have distinctive growth patterns and prognosis (Lal et al., 2017). The heterogeneity of breast cancer is further reflected at the molecular level, tumors that exhibit the same morphological features can express a wide variety of different biomarkers.

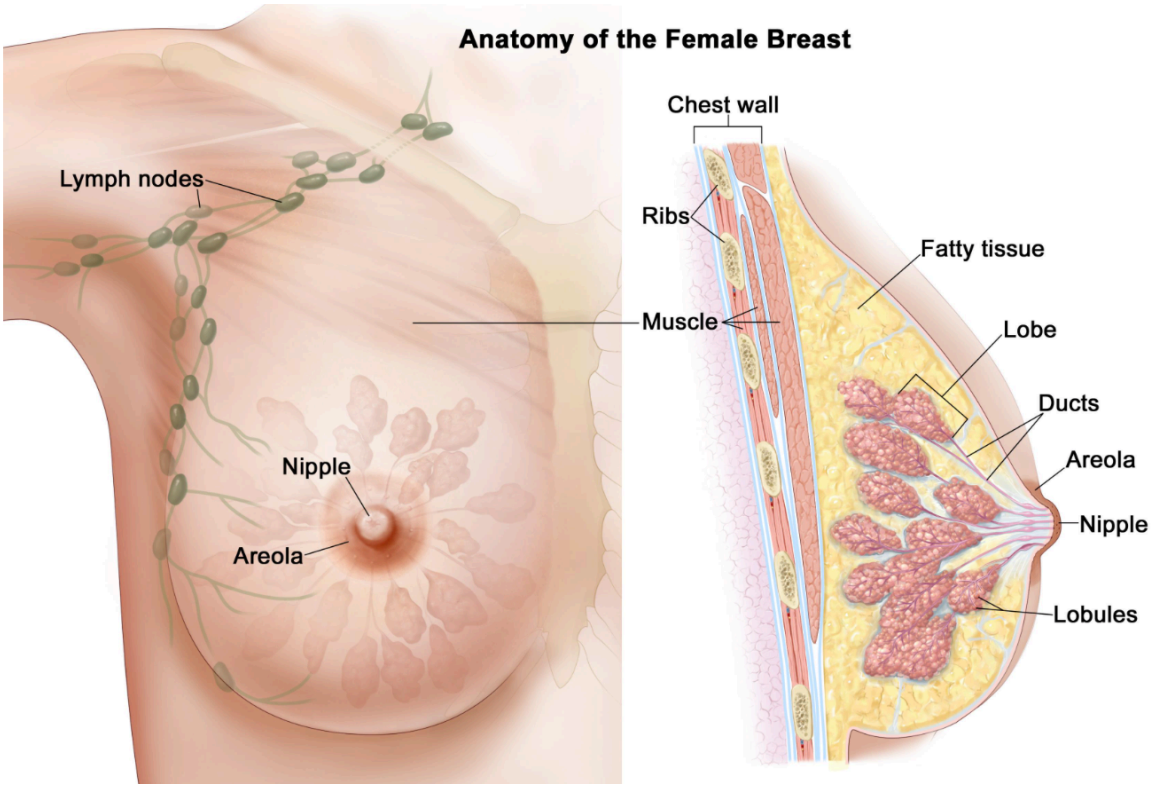

Figure 1.2 Graphical illustration of the anatomy of the female breast

The anatomy of the female breast is illustrated with the nipple, areola and lymph nodes in the left Figure. The right Figure displays a side view cut-through illustration of the anatomical components constituting the female breast. Figure from (nbcf.org.au, 2016).

1.2.1 Breast cancer subtypes

Based on the global gene expression analysis studies by Perou et al (Perou et al., 2000) and Sørlie et al (Sørlie et al., 2001), breast cancer is now recognized as a heterogeneous disease divided into several different molecular subtypes, called the intrinsic subtypes (Prat et al., 2015). The intrinsic subtypes are distinguished by a unique molecular composition, as well as a critical differences in terms of patient outcome, overall survival, prognosis and response to treatment (Sørlie et al., 2001; van 't Veer et al., 2002; Sotiriou et al., 2003; Sørlie, 2004; Wang et al., 2005).

The main intrinsic subtypes (Luminal A, Luminal B, HER2-enriched and basal-like) each exhibit a unique pattern of biomarker expression, which in combination makes up a protein-based signature distinguishing between the different subtypes (Lal et al., 2017). The most common breast cancer biomarkers include estrogen receptor (ER),

progesterone receptor (PgR), human epidermal growth factor receptor 2 (HER2) and the cell-cycle specific antigen Ki-67, which is used as a proliferative marker (Goldhirsch et al., 2013; Cho, 2016; Lal et al., 2017).

As the intrinsic subtypes display differences in treatment response, the 12th St. Gallen International Breast Cancer Conference Expert Panel recommended systemic therapies based on these subtypes (Goldhirsch et al., 2011). For practical purposes the detection of the ER, PgR, HER2 and Ki-67 biomarkers by immunohistochemistry (IHC) were adopted as a convenient approximation to the intrinsic subtypes, resulting in the clinico-pathological surrogate definitions (Luminal A-like, Luminal B-like, HER2 positive and Triple-negative) (Table 1.1).

Luminal A-like breast cancer

Luminal A-like tumors account for approximately 25% of all breast cancer incidents and are defined as ER-positive, PgR-positive and HER2-negative with a low Ki-67 expression (Goldhirsch et al., 2013; Shaoxian et al., 2017) Luminal A-like breast cancer is regarded as a treatable disease with a better prognosis and lower relapse rate than the other subtypes (Eroles et al., 2012). The luminal A-like subtype is an endocrine sensitive breast cancer, treatment of this subgroup is mainly based on anti-estrogen treatment and hormone aromatase inhibitors for postmenopausal patients (Eroles et al., 2012; Rivenbark et al., 2013).

Luminal B-like breast cancer

Luminal B-like breast cancer accounts for approximately 48% of all breast cancer incidents (Shaoxian et al., 2017). The Luminal-B-like subtype is divided into a HER2-positive and a HER2-negative subtype with high Ki-67 expression, both of which are however ER-positive (Goldhirsch et al., 2013). Compared to the luminal A-like subtype the luminal B-like subtypes have a more aggressive phenotype and a worse prognosis, partly explained by a lower response to anti-estrogen therapy (Eroles et al., 2012; Rivenbark et al., 2013). The ER, PgR and HER2-positive subtype of luminal B-like breast cancer is referred to as triple-positive (Vici et al., 2015). Triple positive breast cancer accounts for approximately 10% of all tumors expressing hormonal receptors (ER and PgR). Preclinical evidence has shown that cross-talk between HER2 and ER signalling

pathways may contribute to resistance to endocrine therapy, and consequently a worsening in the patient prognosis (Vici et al., 2015). However, recent advances in HER2 blocking agents and the dual targeting of both hormonal and HER2-pathways have resulted in prolonged survival for patients suffering from this breast cancer subtype. The systemic therapy recommendations for both of the luminal B-like subtypes includes endocrine and chemotherapy, in addition to anti-HER2 therapy for the HER2-positive luminal B-like subtype (Goldhirsch et al., 2013).

HER2-positive breast cancer

Approximately 12% of breast cancer incidents are of the HER2-positive subtype (Shaoxian et al., 2017). This subtype is characterized by the activation of the HER2 oncogene, resulting in the overexpression of HER2 receptor and genes associated with the HER2 amplicon located in the 17q21 chromosome (Eroles et al., 2012; Yersal and Barutca, 2014). Overexpression of HER2 causes tumor growth by constitutive activation of the Ras/Raf/MAPK, JAK/Stat and PI3K/AKT/mTOR pathways, resulting in enhanced cell proliferation, invasion and metastasis (Eroles et al., 2012; Nicolini et al., 2018). HER2-positive tumors have an aggressive phenotype and are typically both ER- and PgR-negative, thus lacking responsiveness to endocrine therapy, resulting in a poor prognosis (Eroles et al., 2012; Rivenbark et al., 2013). However, the HER2-positive subtype has a higher chemosensitivity than the luminal subtypes (Eroles et al., 2012). In addition, research within HER2-targeting agents during the last decade has resulted in substantially improved anti-HER2 treatment. Thus, the recommended systemic therapies for HER2-positive breast cancer consists of cytotoxics and anti-HER2 therapy (Goldhirsch et al., 2013).

Triple-negative breast cancer

Triple-negative breast cancer (TNBC) is a heterogeneous disease defined by the absence of estrogen receptors (ER) and progesterone receptors (PgR) and the absence of HER2 overexpression (Collignon et al., 2016). TNBC accounts for approximately 15% of breast cancer incidents (Collignon et al., 2016; Shaoxian et al., 2017). TNBC has an aggressive clinical behaviour, complex genomic landscape and a higher risk of both local and distant relapse compared to the other subtypes (Collignon et al., 2016; Geyer et al., 2017). The poor prognosis of TNBC is attributed to its vast heterogeneity in addition to

the lack of targetable biomarkers (Bianchini et al., 2016). Interestingly, TNBC generally displays high responsiveness to chemotherapy, which currently is the only systemic treatment option for this disease (Collignon et al., 2016). However, despite optimal systemic chemotherapy less than 30% of patients with metastatic breast cancer, which is a common feature of TNBC, will survive more than 5 years after diagnosis (Bianchini et al., 2016). The breast cancer model used in this thesis is of the TNBC subtype.

Table 1.1 Surrogate definitions of intrinsic breast cancer subtypes according to St. Gallen 2013 International Expert Consensus (Goldhirsch et al., 2013).

Intrinsic subtype	**Clinico-pathologic surrogate definition**				
	Surrogate subtype	*ER*	*PgR*	*HER2*	*PI (Ki67)*
Luminal A	Luminal A-like	+	≥20%	-	<20%
Luminal B	Luminal B-like (HER2-negative)	+	<20%*	-	≥20%*
	Luminal B-like (HER2-positive)	+	Any	+	Any
HER2-enriched	HER2-positive	-	-	+	Any
Basal-like	Triple-negative	-	-	-	Any

ER: Estrogen receptor; PgR: Progesterone receptor; HER2: Human epidermal growth factor 2; PI: Proliferation index; +: Positive; -: Negative; *: Only one of these criteria must be met to define luminal B-like (HER2-negative) breast cancer. Table modified from (Fulawka and Halon, 2017).

1.3 Angiogenesis

Oxygen and nutrients are distributed throughout the body by an extensive network of blood vessels (Logsdon et al., 2014). This vascular network is a dynamic system where the arterioles, venules and capillaries can be extended or expanded in response to stimuli from physiological and pathophysiological events. The growth of new blood vessels from pre-existing vessels is called angiogenesis. This remodelling mechanism is essential for the vascular network during physiological processes such as reproduction, embryogenesis, organ differentiation and tissue repair (Hoff and Machado, 2012; Logsdon et al., 2014).

Angiogenesis also represents an essential step in cancer progression (Yang et al., 2013). In the initial avascular stage of tumor growth, oxygen and nutrients can be obtained through diffusion from nearby blood vessels (within 100 μm) (Yang et al., 2013; Challapalli et al., 2017). However, further expansion beyond the diffusion limitation requires formation of new vasculature (Yang et al., 2013). Tumor cells stimulate angiogenesis by releasing pro-angiogenic factors in the surrounding tissue, which induces the growth of new vasculature to support tumor expansion (Figure 1.3) (Yang et al., 2013; Loizzi et al., 2017). The main pro-angiogenic factors are vascular endothelial growth factor (VEGF), platelet-derived growth factor (PDGF), fibroblast growth factor (FGF), epidermal growth factor (EGF), transforming growth factor (TGF), matrix metalloproteinases (MMPs), tumor necrosis factor (TNF) and angiopoietins (Loizzi et al., 2017).

Tumor angiogenesis lacks the tight regulation and hierarchical ordered patterning which characterizes embryonic angiogenesis (Farnsworth et al., 2014). The vessels of tumor angiogenesis are typically heterogeneous, tortuous, poorly or irregularly branched and often hyperpermeable. The leaky tumor vasculature increases the interstitial pressure, impairs delivery of oxygen and nutrients as well as removal of metabolites. This poorly perfused tumor microenvironment is associated with hypoxia and acidosis, which selects for apoptosis-resistant and metastasis-competent tumor cells and reduces efficiency of radiotherapy. In addition, the increased vascular leakiness and abnormal blood flow in tumors also impairs the delivery of chemotherapeutic drugs (Farnsworth et al., 2014; Kim et al., 2017).

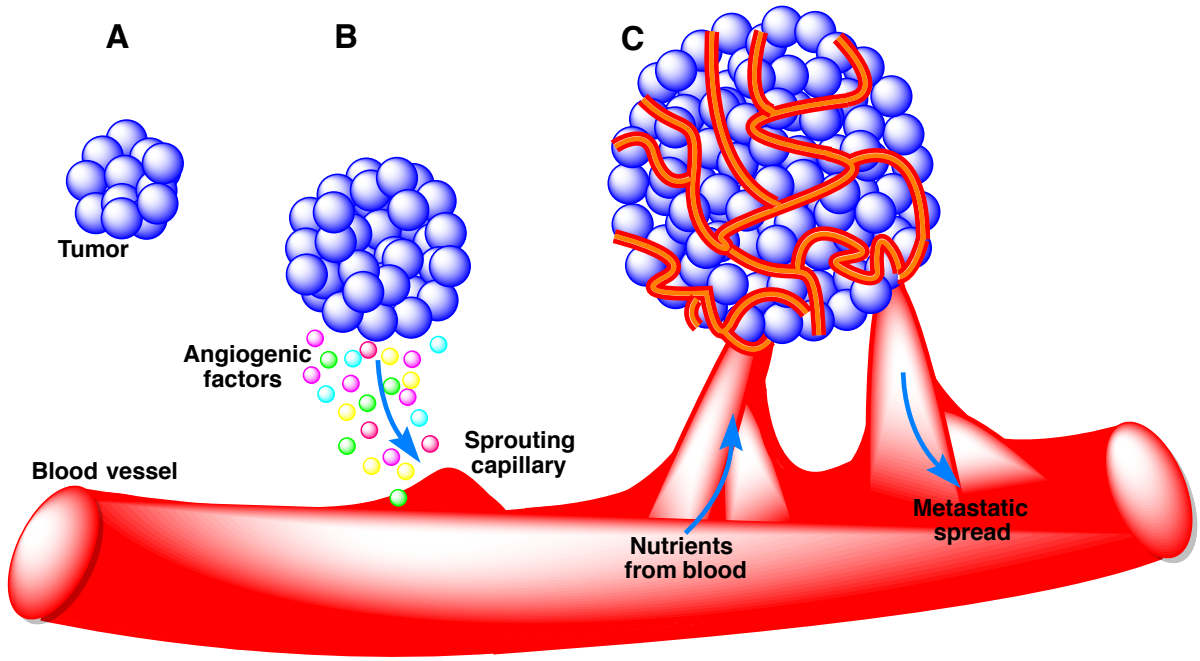

Figure 1.3 Tumor angiogenesis

Graphical illustration of tumor angiogenesis. The tumor expansion proceeds from a small tumor (a) to an invasive tumor (C) through the secretion of pro-angiogenic factors, which stimulate the growth of new vasculature (b). Figure modified from (Loizzi et al. 2017).

1.4 The normal interstitium

The interstitium or interstitial space is a general term for the connective and supporting tissue located between the blood and lymphatic vessels and parenchymal cells (Wiig and Swartz, 2012). The interstitium can be divided into two phases: the interstitial fluid, and the structural molecules constituting the extracellular matrix (Haslene-Hox et al., 2013). Together these two phases comprise the tissue microenvironment.

1.4.1 The extracellular matrix

The extracellular matrix (ECM) is a complex and dynamic network of macromolecules that surrounds cells in all tissues, providing structural and mechanical support (Muiznieks and Keeley, 2013). In addition, the ECM also initiates essential biochemical and biomechanical cues required for tissue morphogenesis, differentiation and homeostasis (Frantz et al., 2010). The macromolecular composition and structural architecture of the ECM is tissue-specific, generated through a dynamic and reciprocal,

biochemical and biophysical dialogue between the various cellular components as well as the evolving microenvironment (Frantz et al., 2010; Muiznieks and Keeley, 2013).

The ECM is composed of proteins and polysaccharide which is synthesised by surrounding cells (e.g. fibroblasts, epithelial and endothelial cells) and secreted into the interstitial matrix (Frantz et al., 2010; Cox and Erler, 2011). The main components of the ECM can be divided into two classes of macromolecules: proteoglycans (PGs) and fibrous proteins such as collagens, elastins, fibronectins, and laminins (Frantz et al., 2010).

1.4.1.1 Collagen

Collagen is the most abundant protein in multicellular animals and the predominant form of structural protein within the interstitial ECM (Frantz et al., 2010). Collagens are mainly synthesized by fibroblasts and secreted in the ECM, where they are providing tensile strength, regulate cell adhesion, support chemotaxis and migration, and direct tissue development.

The collagen family is a heterogeneous family of ECM glycoproteins, consisting of 28 different members (Exposito et al., 2010). All collagen molecules are composed of three α-chains, which consist of a repeating amino acid triplet, Gly-X-Y, where Gly represents glycine, and position X and Y can be any residue but are commonly proline and 4-hydroxyproline, respectively (Theocharis et al., 2016). The three α-chains, which each display a left-handed polyproline II-type conformation, intertwine with a one-residue stagger to form a homo- or heterotrimeric right-handed triple helix, stabilized by interchain hydrogen bonds. This triple helical domain is a characterizing feature shared by all collagens.

According to their common domain homology and functions the collagens can be classified as fibrillar collagens, network-forming collagens, FACITs (fibril-associated collagens with interrupted triple helices), MACITs (membrane-associated collagens with interrupted triple helices), anchoring fibrils, beaded filament-forming collagens, and MULTIPLEXINs (multiple triple-helix domains and interruptions)(Theocharis et al.,

2016). The fibrillar collagens (type I-III, V, XI, XXIV and XXVII), particularly type I collagen, are the most abundant collagens (Gelse et al., 2003; Exposito et al., 2010).

1.4.1.2 Fibroblasts

Fibroblasts are the most common cell type of the connective tissues throughout the body, and the primary source of the ECM´s structural and adhesive proteins, and ground substance (Kendall and Feghali-Bostwick, 2014). In addition, fibroblasts play pivotal roles in a multitude of physiological and pathological events, including ECM maintenance and remodelling, wound healing, inflammation, angiogenesis, cancer progression and fibrosis.

The fibroblasts are embedded into the ECM and subjected to a variety of chemical and physical stimuli, such as tension, compression and shear stress (Wang et al., 2007). Through cell surface receptors, such as integrins, the fibroblasts are capable of interacting and communicating with their surroundings (Alkasalias et al., 2018). This intimate connection with their surroundings, enable fibroblasts to display high sensitivity and responsiveness to different external stimuli (Kendall and Feghali-Bostwick, 2014). To this effect, the fibroblasts are essential in maintaining normal tissue architecture in a dynamic cellular environment, and as critical contributors in the ECM remodelling in a range of pathological conditions (Kendall and Feghali-Bostwick, 2014; Alkasalias et al., 2018).

The fibroblastic cell type is not terminally differentiated, thus the fibroblasts retain the potential for differentiation into myofibroblasts if activated by chemical and physical stimulation, such as wound healing, mechanical stress or in response to cytokines (Kendall and Feghali-Bostwick, 2014; Falke et al., 2015). The myofibroblast (Figure 1.4) phenotype is characterized by expression of α-smooth muscle actin, increased contractile properties, excessive production of ECM molecules and elevated expression of cytokines, chemokines, growth factors and cell surface receptors (Baum and Duffy, 2011; Kendall and Feghali-Bostwick, 2014).

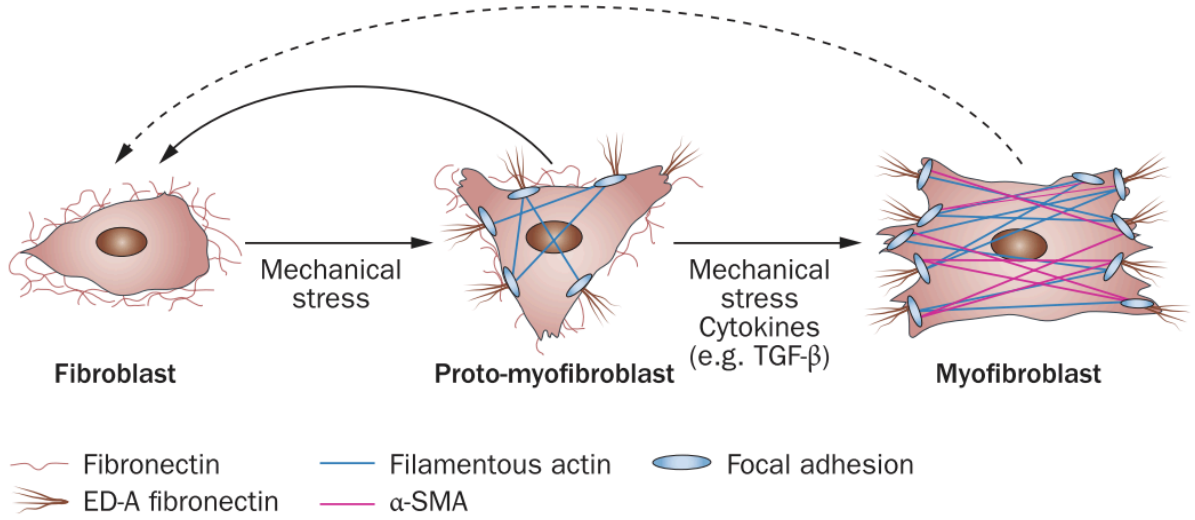

Figure 1.4 Myofibroblast differentiation

The Figure displays the difference in contractile properties during the differentiation steps from fibroblast to myofibroblast. Myofibroblasts express α-smooth muscle actin and display increased contraction of focal adhesions in response to mechanical stress and cytokines, such as TGF-β. The transition between proto-myofibroblast and fibroblast is reversible (solid arrow), while the transition between myofibroblast and fibroblast is unknown (dotted arrow). Figure from (Falke et al., 2015) with permission.

1.4.2 The interstitial fluid and transcapillary exchange

The interstitial fluid is an extracellular liquid created as a result of a continuous flow of fluid and solutes from the vascular system to the lymphatic system for subsequent reabsorption (Scallan et al., 2010, pp. 21-33). Thus, the interstitial fluid represents the interface between the parenchymal cells in a tissue and the circulatory system, mediating the exchange of oxygen, nutrients and waste products (Heldin et al., 2004; Pittman, 2013).

The movement of fluids across the capillary wall is governed by the hydrostatic and colloid osmotic pressure gradients in the blood vessels and the interstitial space, collectively referred to as the Starling´s forces (Heldin et al., 2004; Baronzio et al., 2012). The hydrostatic pressure in each of these compartments exerts a pushing force across the vessel wall, attempting to move fluid out (Sawdon and Kirkman, 2017). Whereas the osmotic pressure contributed by the protein concentrations in the blood and interstitial space exert a suction force or absorptive force, which attempts to draw fluid in (Levick,

2010, pp. 188-191; Sawdon and Kirkman, 2017). The net imbalance in these pressure gradients determines the direction and magnitude of the transcapillary filtration (Heldin et al., 2004). At normal physiological conditions, there is a net outwards filtration pressure from the capillaries, which enable the transport of nutrients and waste products between cells and the circulatory system.

Along with properties of the capillary wall, the Starling´s forces constitute the basic principles for fluid exchange described by Starling (Starling, 1896) over a century ago (Wagner and Wiig, 2015). The Starling principle of fluid exchange is mathematically described by the Starling equation (Eq. 1.1) (Baronzio et al., 2012).

$$J_v = L_p S\,[(P_{cap} - P_{if}) - \sigma(COP_{cap} - COP_{if})] \qquad \text{(Eq. 1.1)}$$

Where J_v is the volume flux of fluid; L_p is the hydraulic conductivity; S is the surface area available for filtration; P_{cap} and P_{if} is the capillary and interstitial hydrostatic pressures, respectively; COP_{cap} and COP_{if} is the capillary and interstitial colloid osmotic pressures, respectively; and σ is the osmotic reflection coefficient of the vessel wall, which ranges from 0 (freely permeable to proteins) to 1 (completely impermeable to proteins) (Baronzio et al., 2012).

1.5 The tumor interstitium

Remodelling and stiffening of the ECM is a characterising feature of most solid tumors, especially in breast tumors (Levental et al., 2009). Fibroblasts, which are key regulators of the ECM composition and organization, tend to acquire a constantly activated phenotype in tumors as a response to high mechanical tension and secreted growth factors (Northey et al., 2017; Kalli and Stylianopoulos, 2018). These cancer-associated fibroblasts are most commonly defined by expression of α-smooth muscle actin and the acquisition of a phenotype resembling myofibroblasts (Hanley et al., 2018). Upon activation, the myofibroblasts initiate a chronic wound healing-like response resulting in excessive accumulation of fibrillar ECM proteins (Figure 1.5), a process as desmoplasia (Kalli and Stylianopoulos, 2018). Importantly, increased collagen deposition during the

tumor-induced desmoplastic response, upregulates the expression and activity of the collagen-crosslinking enzyme, lysyl oxidase (LOX) (Handorf et al., 2015). LOX-mediated collagen crosslinking further increases ECM stiffness and is directly linked to aggression and invasiveness in mammary tumors (Northey et al., 2017).

The excessive ECM remodelling during tumor-induced desmoplasia reshapes the physical properties of the tumor microenvironment (Alkasalias et al., 2018). Increased ECM stiffness exerts a physical force on the surrounding cells, a force sensed through integrin adhesions (Gehler et al., 2013). The cells respond to the external force by increasing the actomyosin contractile forces to maintain the structural integrity. To this effect, ECM stiffness induces integrin-mediated actin cytoskeletal reorganization and contractility, thus influencing cell-matrix adhesion, migration, cell-cycle progression and differentiation (Handorf et al., 2015).

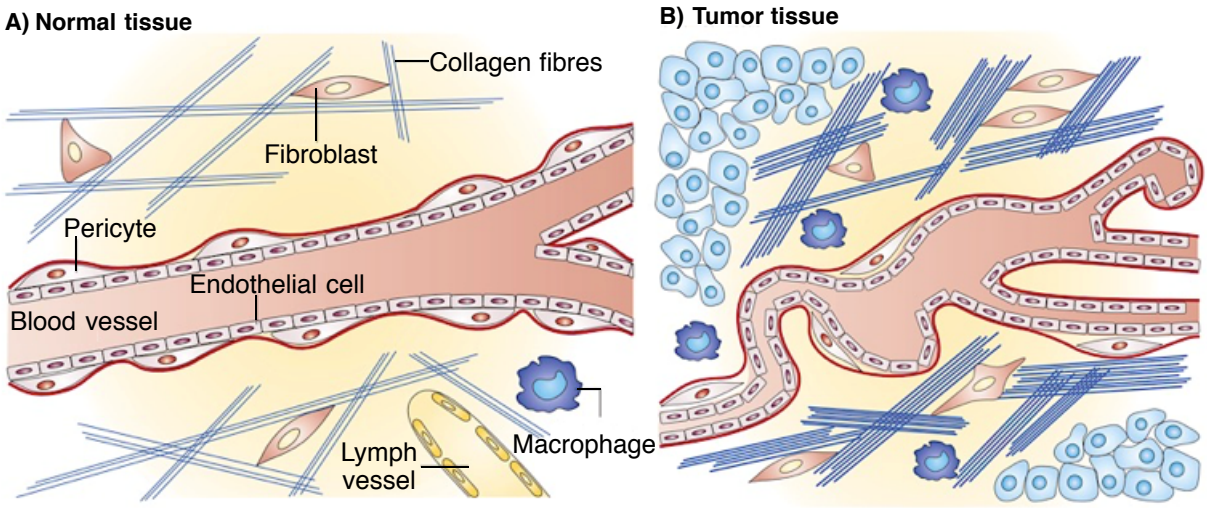

Figure 1.5 Interstitium composition in normal tissue and tumor tissue

A) Normal tissue contains linear blood vessels lined with endothelial cells covered by pericytes. The extracellular matrix consists of a loose network of collagen and other fibres in addition to a few fibroblasts and macrophages. Lymph vessels are present and functional. B) Tumor tissue contains leaky and irregular shaped blood vessels with low pericyte coverage. Many tumors also lack lymph vessels, resulting in insufficient drainage of interstitial fluid. Tumors contain a denser extracellular matrix, mainly composed of collagen fibres. Fibroblast are also present in higher number, these bind to collagen fibres in an integrin-dependent manner and exert an increased tension. The amount of macrophages and other inflammatory cells are also elevated; these cells release cytokines and growth factors that act on endothelial cells and stromal fibroblasts, resulting in elevated interstitial pressure. Figure adapted from (Heldin et al., 2004) with permission.

In addition, increased ECM density acts in concert with other tumor properties such as high vascular permeability and impaired lymphatic function to elevate the interstitial hydrostatic and colloid osmotic pressures (Heldin et al., 2004; Butcher et al., 2009). This shift in the transcapillary pressure gradients (Figure 1.6) impede the convective transport into tumors (Heldin et al., 2004). In normal tissue, the net imbalance in the Starling´s forces ensures an outwards flow of fluids from the capillaries into the interstitium. High interstitial fluid pressure, which is a common feature in most solid tumors alters the normal pressure gradients and thus impede the normal transcapillary transport. Importantly, high interstitial fluid pressure creates a pressure barrier that impairs the uptake and distribution of systemically administered anti-cancer drugs.

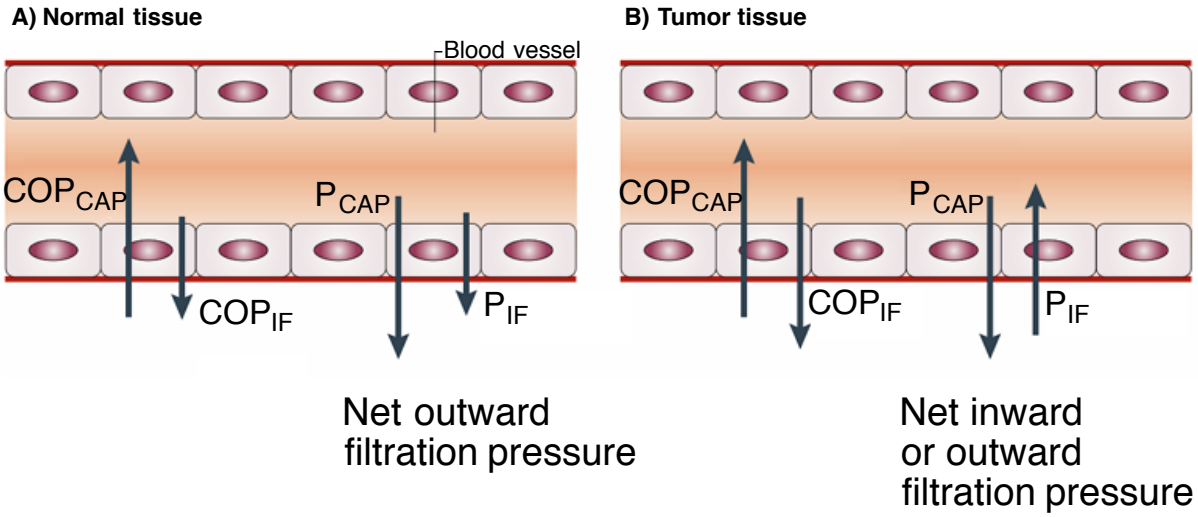

Figure 1.6 Starling´s forces in the regulation of transcapillary exchange

COP_{cap} is the capillary colloid osmotic pressure, COP_{if} is the interstitial colloid osmotic pressure, P_{cap} is the capillary hydrostatic pressure, and P_{if} is the interstitial hydrostatic pressure. The direction of the arrows represents the pressure direction and the sizes of the arrows indicate the force of the pressure. A) In normal tissue the Starling´s forces assure a net outward filtration pressure from the capillaries into the interstitium. B) In tumor tissue, increased ECM density acts in concert with increased blood vessel permeability and lacking lymphatic drainage to elevate the interstitial oncotic pressure and the interstitial hydrostatic pressure (Heldin et al., 2004). The alteration of the pressure gradients in the Starling´s forces impedes the physiological transcapillary exchange, creating a pressure barrier that opposes the uptake and distribution of systemically administered anti-cancer. Figure adapted from (Heldin et al., 2004) with permission.

1.6 Integrins

Integrins are a large family of cell surface receptors which mediate cell-matrix and cell-cell adhesions (Ramage, 2012). In addition, these receptors also provide a mechanical link between the cells external and internal environment, enabling cells to detect and adapt to changes in the biophysical properties of the extracellular milieu (Ramage, 2012; Sun et al., 2016).

The integrins are transmembrane heterodimers composed of non-covalently associated α and β subunits (Harburger and Calderwood, 2009). The mammalian genome contain 18 α subunits and 8 β subunits, which combine to form 24 distinct integrins (Humphries et al., 2006). Based on their ligand recognition pattern, the integrin family of receptors can be broadly classified into four different categories: the RGD receptors, the collagen receptors, the laminin receptors and the leukocyte-specific receptors, as shown in Figure 1.7 (Goswami, 2013).

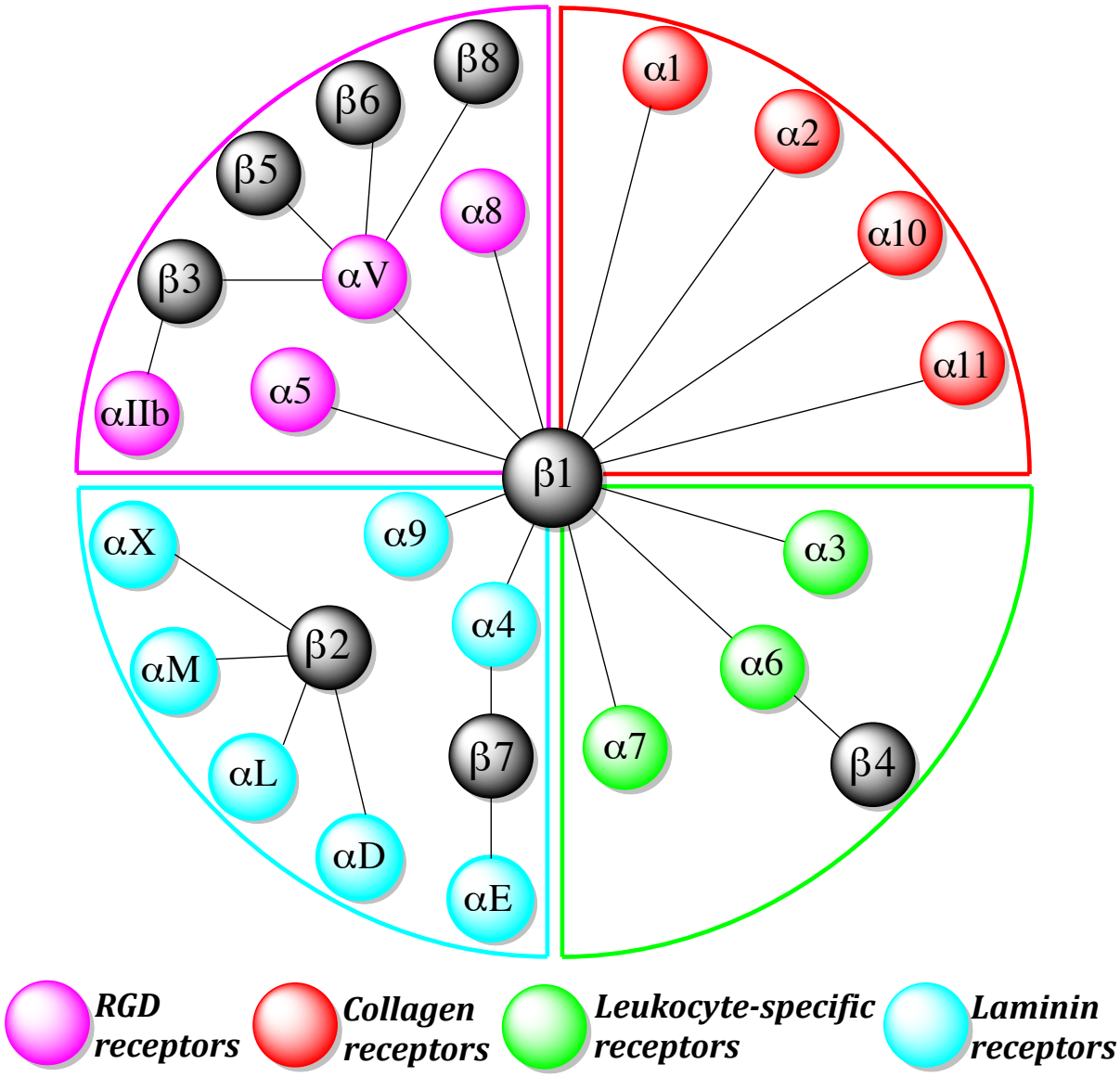

Figure 1.7 The integrin receptor superfamily

The Figure displays the human integrin superfamily and how the α and β subunits combine to form the heterodimeric integrin receptors. The members of the integrin superfamily can be categorized into four categories according to their ligand recognition pattern (Goswami, 2013). Figure modified from (Barczyk et al., 2010).

The integrin heterodimer consists of a large extracellular domain that binds proteins in the extracellular environment, a single transmembrane domain, and a short cytoplasmic tail, which forms links with the cytoskeletal elements through cytoplasmic adaptor proteins (Srichai and Zent, 2010, pp. 19-36). This physical link between the extracellular environment and the actin cytoskeleton allows bi-directional signalling across the plasma membrane, as shown in Figure 1.8.

Integrin activation by ECM ligands (outside-in signalling) induces a conformational change in the integrin structure, and promotes integrin clustering due to the multivalent nature of many ECM ligands (Shattil et al., 2010). The combination of these events results in intracellular signalling cascade that regulate cell polarity, survival and migration, changes in cytoskeletal structure and gene expression (Mas-moruno et al., 2010; Shattil et al., 2010).

The other type of integrin activation (inside-out signalling) occurs through intracellular activators, such as talin or kindlins (Shattil et al., 2010). These activators bind to the cytoplasmic tail of the β-subunit, inducing a conformational change that increases the integrins affinity for extracellular ligands. This process regulates the adhesive strength of the integrin-ECM interaction, allowing the necessary force transmission for cell migration and ECM remodelling.

In addition, the presence of unligated integrins trigger the activation of caspase-8 and consequently apoptosis through a mechanism called integrin-mediated death (IMD) (Mas-moruno et al., 2010).

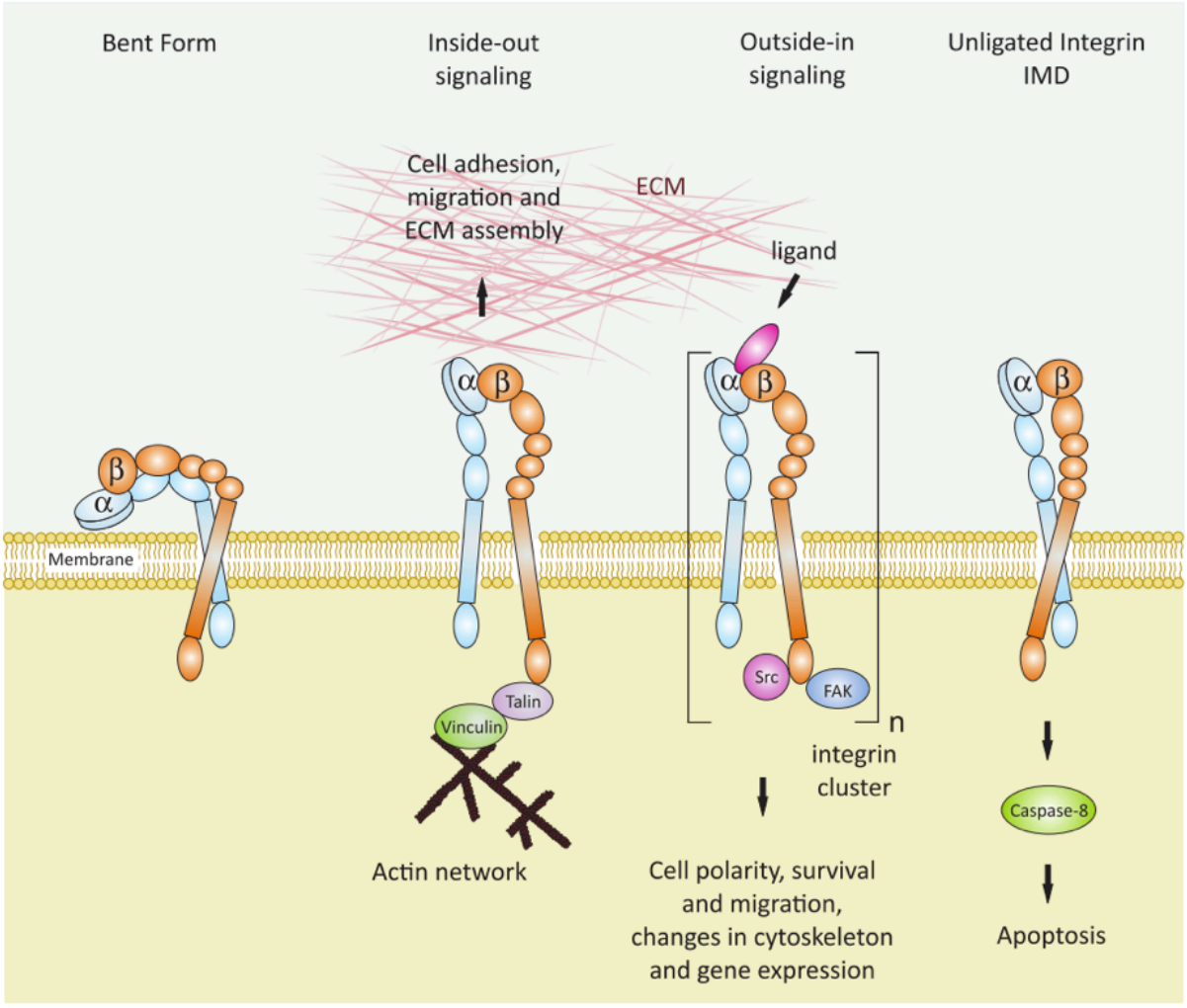

Figure 1.8 Integrin activation states and signalling mechanisms

In the bent form, the integrin head group point towards the cell surface and the receptor displays low affinity towards ligands (Mas-moruno et al., 2010). During "inside-out signalling" intracellular activators, such as talin or kindlins, bind to the cytoplasmic tail of the β-subunit and induces a conformational change leading to increased affinity for extracellular ligands. This process regulates cell adhesion, migration and invasion. During "outside-in signalling" binding of ECM ligands induces change in conformation and integrin clustering due to ligand multivalency. This type of integrin activation results in an intracellular signalling cascade that regulate cell polarity, survival and migration, changes in cytoskeletal structure and gene expression. The presence of unligated integrins can activate caspase-8 and consequently the induction of apoptosis, in a process called integrin-mediated death (IMD). Figure from (Mas-moruno et al., 2010) with permission.

Integrins are central to the biology of a wide range of human pathologies, including fibrosis, thrombosis, inflammation and cancer (Raab-Westphal et al., 2017). In the setting of cancer, the important biological roles of integrins can be exploited by tumor cells to promote invasiveness, oncogenic survival and to engineer a microenvironment

that is conductive of tumor growth and metastatic spread (Hamidi et al., 2016). The integrins accessible exposure on the cell surface in addition to increased expression in pathological conditions, has landed them as seductive therapeutic targets (Raab-Westphal et al., 2017).

1.6.1 Integrin α11β1

Integrin α11β1 is a collagen-binding integrin, a feature sheared with three other integrins, α1β1, α2β1, and α10β1 (Zeltz and Gullberg, 2016). Together these four integrins constitute the collagen-binding family of the integrin receptors. Integrin α11β1 was the latest addition to this family, characterized in 1999 (Velling et al., 1999) following the identification of its α-chain in 1995 by Gullberg and colleagues (Gullberg et al., 1995).

Integrin α11β1 expression is primarily restricted to a subset of fibroblasts and to mesenchymal stem cells (Zeltz and Gullberg, 2016). Integrin α11β1 has high affinity for collagen type I, and has been reported as the main collagen receptor expressed on fibroblasts within the tumor stroma (Schnittert et al., 2018). Integrin α11β1 contributes to TGF-β-dependent collagen remodelling and myofibroblast differentiation (Zeltz and Gullberg, 2016; Schnittert et al., 2018).

In addition, the involvement of integrin α11β1 in collagen remodelling, specifically collagen-crosslinking and stromal stiffness, has been suggested to be conductive of an invasive tumor phenotype (Navab et al., 2016). Importantly, Navab and colleagues showed that the incidence of systemic metastasis of non-small cell lung cancer (NSCLC) to bone, brain, kidneys, lymph nodes, and opposite lung was significantly lower in $\alpha 11^{+/-}$ and $\alpha 11^{-/-}$ mice compared to $\alpha 11^{+/+}$ mice.

1.7 Platelet-derived growth factors and their receptors

The PDGF system is composed of five homo- or heterodimeric ligands (PDGF-AA, PDGF-AB, PDGF-BB, PDGF-CC and PDGF-DD) and two receptor tyrosine kinases (PDGFRα and PDGFRβ), which either homo- or hetero-dimerize upon ligand binding (Östman, 2017; Heldin et al., 2018). The PDGF ligands displays different affinity for the receptors, thus PDGF-AA, PDGF-AB, PDGF-BB and PDGF-CC induce αα-homodimeric receptor complexes (Heldin et al., 2018). The PDGF-BB and PDGF-DD ligands induce ββ-homodimeric receptor complexes, while PDGF-AB, PDGF-BB, PDGF-CC and PDGF-DD induces the αβ-heterodimeric receptor complexes, as shown in Figure 1.9.

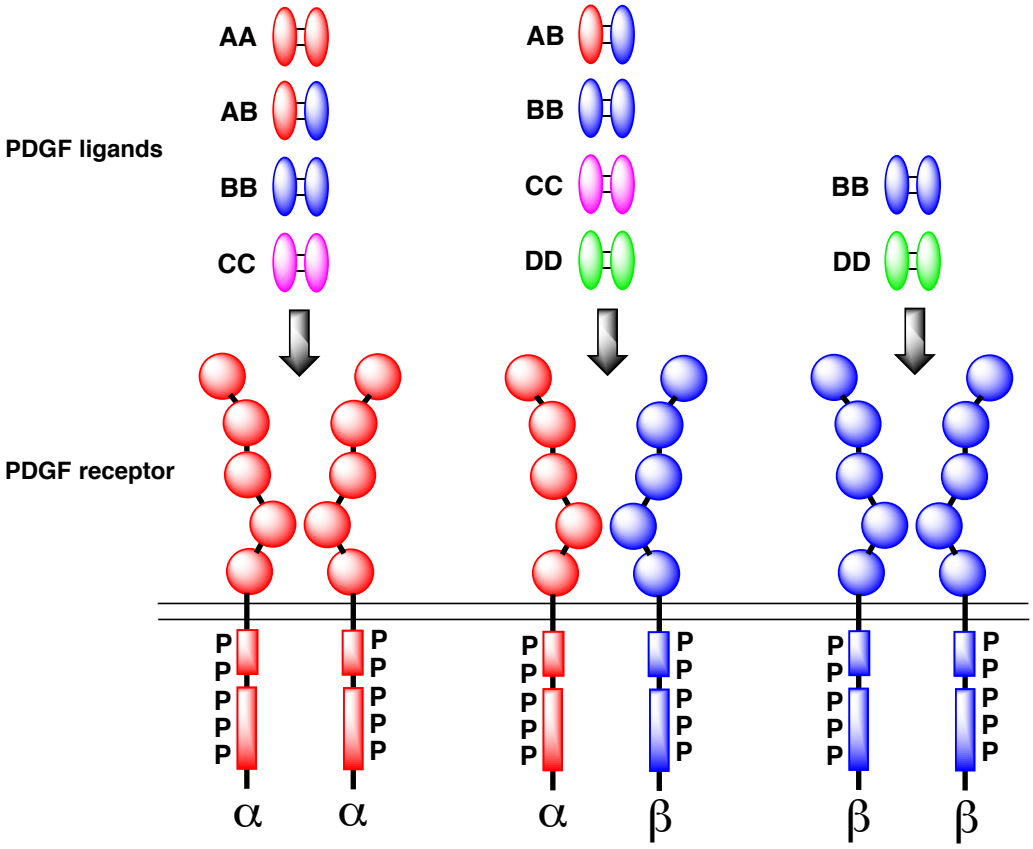

Figure 1.9 Overview of the PDGF system

The PDGF ligands (PDGF-AA = red, PDGF-AB = red and blue, PDGF-BB = blue PDGF-CC = magenta and PDGF-DD = green) bind to the extracellular domains (red or blue circles) of the receptors. Ligand binding induces receptor dimerization (PDGFR-αα = red, PDGFR-αβ = red and blue, and PDGFR-ββ = blue) and autophosphorylation (P) on the receptors intracellular kinase domains (red or blue rectangles), creating docking sites for SH2-domain-containing signalling molecules. Activation of these signalling pathways promotes cell growth, survival, migration and actin reorganization (Heldin, 2013). Figure modified from (Heldin, 2013) with permission.

The PDGF ligands are members of the cysteine-knot protein superfamily (Chen et al., 2013). The defining feature of this protein family is a conserved growth factor domain in the cysteine-knot fold, which is primarily responsible for recruiting receptors. In addition, the cysteine-knot fold offer substantial structural stability and promotes the formation of homo- and hetero-dimers through intermolecular disulphide bridges. The different polypeptide chains of the PDGF isoforms are synthesized as precursor molecules (Heldin, 2014). The A- and B-chains are activated in the trans-Golgi network by proprotein convertases, while the C- and D-chains are processed by extracellular proteases after secretion (Heldin, 2014; Östman, 2017).

The PDGFs are mesenchymal mitogens with important functions during embryonic development and as regulators of the tissue homeostasis and the interstitial fluid pressure in the adult (Heldin, 2014). The PDGF ligands exerts their cellular effects through binding with their cognate receptors (Heldin, 2013). The PDGF receptors are transmembrane receptors, belonging to the type III receptor tyrosine kinase family (Heldin and Lennartsson, 2013).

The extracellular part of the receptor consists of five Ig-like domains. The second and third of the Ig-like domains are responsible for ligand binding, upon binding, receptor dimerization is induced. The resulting dimer is stabilized by direct receptor-receptor interactions in Ig-like-domains four and five. PDGF-induced receptor dimerization brings the intracellular domains in close proximity of each other, promoting autophosphorylation *in trans* between the receptors (Heldin, 2013).

The autophosphorylation serves two important functions. First, it induces a conformational change in the intracellular part of receptors that activate their kinase activity. Secondly, autophosphorylation creates docking sites for downstream SH2-domain-containing signalling molecules and other adaptor molecules, which lack intrinsic enzymatic activities, but capable of forming complexes with signalling molecules. The activation of these signalling pathways leads to cell proliferation, survival, actin reorganization, and cell migration.

1.7.1 PDGFR inhibition

PDGFRs are important regulators of fibroblasts and pericytes, and have been found to regulate multiple aspects of tumor biology including tumor growth, metastasis, immune surveillance as well as the efficiency and uptake of drugs (Östman, 2017). Studies on several different tumor models have demonstrated that inhibition of stromal PDGF receptors reduced tumor interstitial pressure, increased drug uptake and efficiency. Moreover, PDGFs contribute to increased interstitial fluid pressure by promoting integrin-mediated adhesion to ECM proteins and contraction of stromal fibroblasts or myofibroblasts (Heldin et al., 2004, 2018).

The overexpression of PDGFs and their cognate receptors have been reported in a range of human malignancies, and correlates with poorer therapy response and shorter survival (Raica and Cimpean, 2010). A wide variety of therapeutic strategies have been investigated to address the deregulated tyrosine kinase activity. One of the most effective drugs against PDGFRs is imatinib (Gleevec).

Gleevec is a synthetic small-molecule adenosine triphosphate analogue that inhibits phosphorylation of a number of tyrosine kinase receptors including PDGFR, c-kit and bcr-abl (Vlahovic et al., 2007; Raica and Cimpean, 2010) Tyrosine kinases catalyse the transfer of the terminal phosphate group from ATP to tyrosine residues on its substrates, a process known as tyrosine phosphorylation (Iqbal and Iqbal, 2014). Gleevec works by binding close to the ATP binding site on the enzyme, locking it in a closed or self-inhibited conformation, thereby inhibiting the enzymatic activity in a semi-competitive manner, as shown in Figure 1.10.

Gleevec have been shown to significantly inhibit cell growth of breast cancer cells (Roussidis et al., 2007; Weigel et al., 2009). In addition, Malavaki and colleagues showed that Gleevec exerted a significant inhibitory effect on breast cancer cell proliferation, invasion and migration (Malavaki et al., 2013). Inhibition of PDGFs has also been shown to reduce the interstitial fluid pressure and enhance therapeutic effect in experimental models.

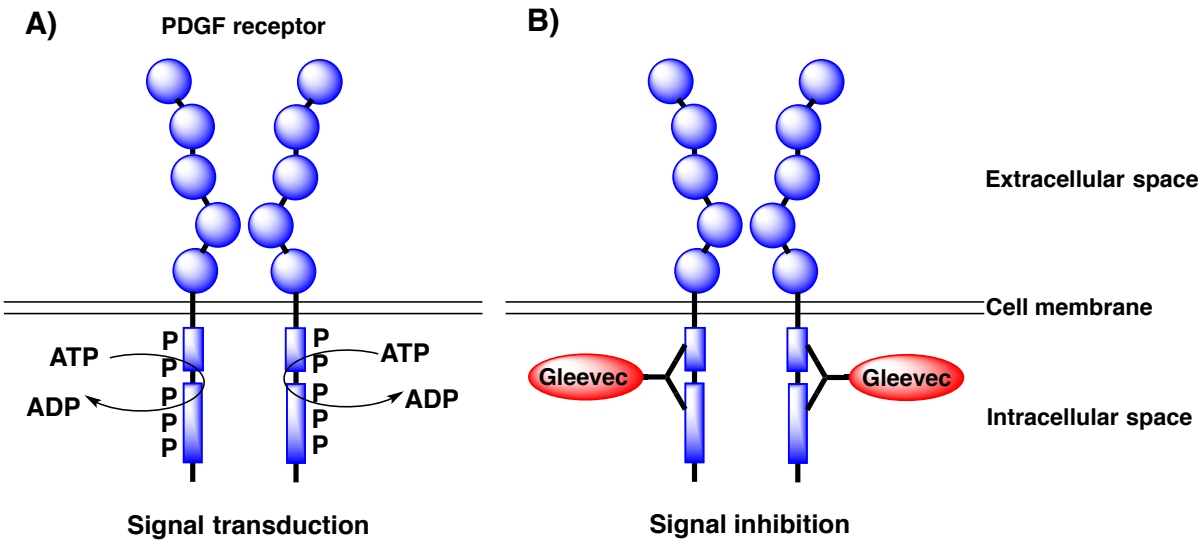

Figure 1.10 PDGFR inhibition

Graphical illustration of PDGFR inhibition by Gleevec. A) PDGF receptors (blue) catalyse the transfer of the terminal phosphate group from ATP to tyrosine residues on its substrates, a process known as tyrosine phosphorylation (Iqbal and Iqbal, 2014). B) Gleevec (red) works by binding close to the ATP binding site on the enzyme, locking it in a closed or self-inhibited conformation, thereby inhibiting the enzymatic activity in a semi-competitive manner. Figure modified from (Savage and Antman, 2002; Heldin, 2013).

2 Aims

The main goal of this thesis was to evaluate the *in vivo* effect of integrin α11-deficiency and PDGF inhibition using the murine E0771 triple-negative breast cancer model. This goal will be addressed through two specific aims.

Aims of this thesis:

1. Evaluate the *in vivo* effect of integrin α11-deficiency on tumor growth, interstitial fluid pressure, angiogenesis, and collagen density in the murine E0771 TNBC model.

2. Evaluate the *in vivo* effect of PDGF inhibition on tumor growth, interstitial fluid pressure, angiogenesis, and collagen density in the murine E0771 TNBC model.

3 Materials and methods

In order to give a clear description of the methods and experimental procedures involved in this thesis, this section will start with a brief overview of the experiment (Figure 3.1). Details will follow subsequently.

In this thesis, 28 SCID mice with and without integrin α11-deficiency (13 α11-KO and 15 WT) were injected with $5x10^5$ E0771 tumor cells in a 0.15 mL PBS suspension into the fat pad of the fourth mammary gland. The integrin α11-deficient mice and the wild type mice were randomly allocated into control groups and experimental groups based on their integrin α11 status. After the tumors reached an appropriate size (approximately 150 mm^3) the experiment were initiated.

The experiment was performed over the course of four days, in which the animals in the control groups received ddH_2O by gavage, while the experimental groups received the tyrosine kinase inhibitor Gleevec by gavage once a day. The initial tumor sizes were measured with a caliper at the start of the experiment. At the experimental end-point the tumor sizes were re-measured followed by measurements of the tumor interstitial fluid pressures using the wick-in-needle technique. After performing these measurements, the animals were sacrificed by cervical dislocation while anaesthetized and the tumors were excised for further analysis.

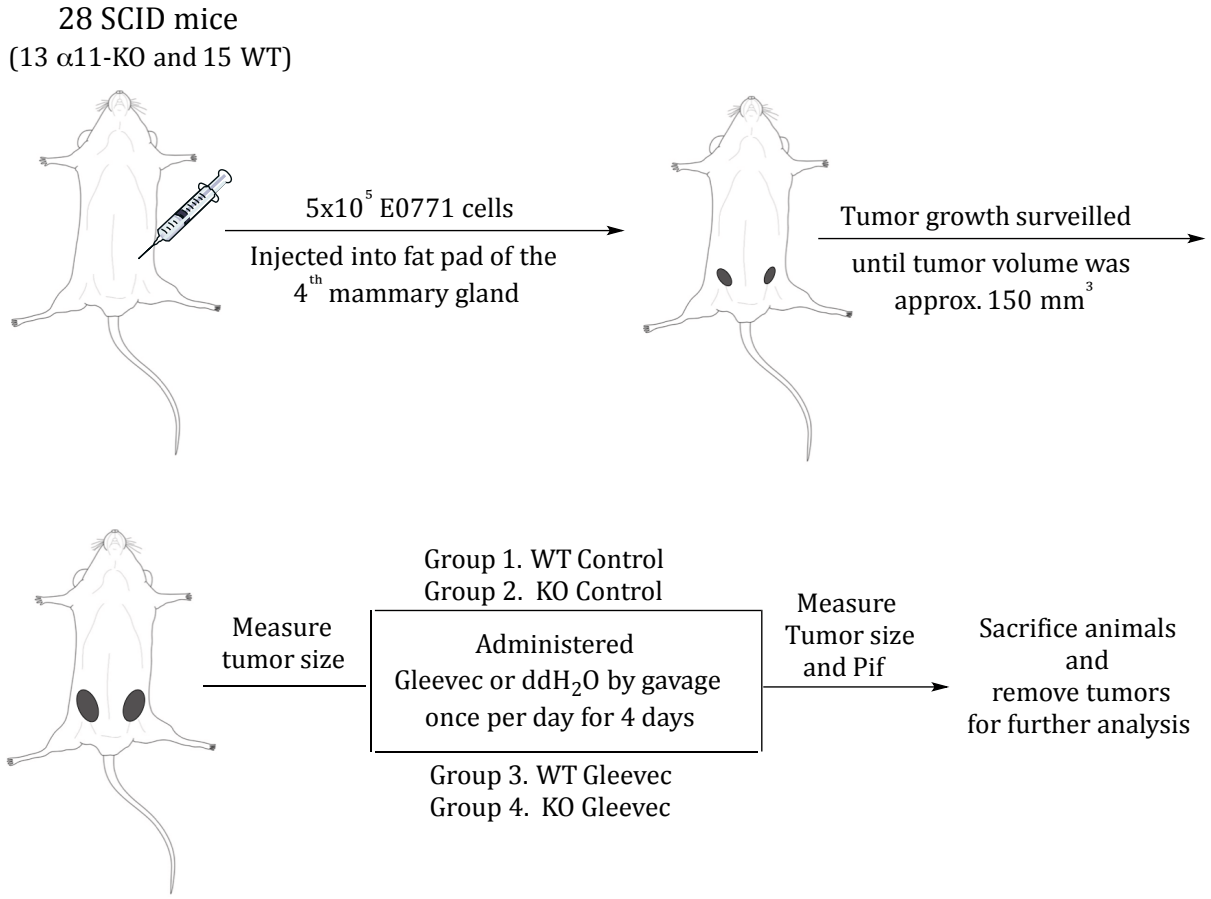

Figure 3.1 Experimental overview.

In this experiment 26 SCID mice (11 α11-KO and 15 WT) were injected with $5x10^5$ E0771 tumor cells in a 0.15 mL PBS suspension into the fat pad of the fourth mammary gland. The growth of the tumors and the health status of the animals were surveyed. When the tumors reached an appropriate size of approximately 150 mm^3 the experiment were initiated. The initial tumor sizes were measured with a caliper and the control groups were administered water by gavage while the experimental groups (Gleevec groups) were administered the tyrosine inhibitor Gleevec by gavage. The animals were treatment over a period of four days. At the endpoint of the experiment, the size of tumors were re-measured followed by measurement of the tumor interstitial fluid pressure. The animals were thereby sacrificed by cervical dislocation and the tumors excised for further analysis.

3.1 Cells

3.1.1 Cell line and culturing

The murine mammary carcinoma cell line (E0771) purchased from CH3BioSystems (940001, CH3BioSystems, New York, USA) was used in this thesis. This cell line was originally isolated from a spontaneous tumor in the mammary gland of a C57BL/6 mouse (Sugiura and Stock, 1952). Immunohistochemical analysis of the E0771 cell line has revealed that it has core basal phenotype, defined as triple-negative breast cancer (Johnstone et al., 2015).

The E0771 cells were cultured in RPMI-1640 medium supplemented with 25 mM HEPES, 10% Fetal Bovine Serum (FBS), 2% L-glutamine, 100 units/mL penicillin and 100 µg/mL streptomycin (all from Sigma-Aldrich, Steinheim, Germany). The cells were grown as a monolayer in filter capped 175 cm^2 cell culture flasks (NUNC, Roskilde, Denmark) in a humidified incubator at 37^{0}C with 5% CO_2 and 95% air and seeded until approximately 75% confluence.

All cell work was performed in a sterile environment using a laminar flow fume hood with a HEPA filter (Thermo Scientific, USA).

3.1.2 Sub-culturing and seeding

For passaging of cells, growth medium was removed and the cells were washed 3 times with 10 mL pre-heated Dulbecco`s Phosphate Buffered Saline (PBS) (Sigma-Aldrich, Steinheim, Germany), 5 mL Trypsine-EDTA (Sigma-Aldrich, Steinheim, Germany) was added followed by incubation for 3 min to allow the cells to detach from the flask and form a single cell suspension. After incubation, the cells were resuspended in 7 mL fresh medium. The new cell suspension was split, and both flasks were added 24 mL fresh medium.

3.1.3 Freezing and thawing

After cell passaging, the cells were transferred to a 15 mL Falcon tube and centrifuged at 900 rpm at 4^0C for 4 min (Eppendorf Centrifuge 5810 R, Hamburg, Germany). The supernatant was carefully discarded and the cells resuspended in 2 mL freezing solution (80% DMEM-ALT, 10% FBS and 10% DMSO) (all from Sigma-Aldrich, Steinheim, Germany). The cell suspension was distributed into two cryotubes wrapped in paper and acclimatized at -80^0C for 24 hours. The cryotubes were then transferred to a nitrogen tank for cryopreservation at -196^0C.

For thawing, the cells were placed in a warm water bath at 37^0C. Immediately after thawing the cells were transferred to a culture flask containing 15 mL DMEM-ALT and placed in an humidified incubator at 37^0C in a 5% CO_2 and 95% air for 24 hours. The following day, the medium was discarded and the cells washed 3 times in 10 mL PBS to remove remnants of freezing solution, which may otherwise harm the cells. Subsequently, new medium was added to the cells.

3.2 Animals

3.2.1 Animal models and housing

A total of 28 female BALB/c SCID mice with an initial weight ranging from 17-25 g were used as models for the E0771 cell line. Of these mice, 13 were integrin α11-deficient (α11-KO). That the mice were homozygous for integrin α11, either WT or α11-KO, was confirmed by PCR-genotyping on DNA extracts from ear biopsies (See Appendix A for protocol). The mice were identified throughout the experiment by labels at the base of their tails with a permanent marker and ear notches.

All mice were housed in intraventilated Makrolon IVC Type IV cages (Techniplast Gazzada, S.a.r.l., Buggigiate, Italia) on soft wooden bedding (Scanbur AS Norway, Norway), with 70 air changes per hour. The animals had access food (Special Diet Service, Witham Essex, UK) and water *ad libitum.* The ambient temperature in the

animal facility was kept within an optimum of 20-21^{0}C, with a relative humidity between 40-60% and an artificial light/dark cycle of 12/12 hours. Health monitoring was performed regularly according to the recommendations of the Federation of European Laboratory Animal Science Associations (FELASA).

All procedures were approved by and performed in accordance with regulations from the Norwegian Committee for Animal Research (The National Animal Research Authority (FOTS) bearing the project ID. 11253). The number of animals used was minimized in compliance with the guidelines from the local Ethical Committee.

3.2.2 Anaesthesia and euthanasia

During tumor measurements the animals were shortly anaesthetized with Isoflurane (IsoFlo®Vet, Zoetis, Helsinki, Finland) combined with N_2O and O_2 gas-anaesthesia. Induction of anaesthesia was performed in a Plexiglas anaesthetic chamber (SurgiVet®, Smiths medical, Norwell, Massachusetts, USA) flushed with N_2O and O_2 at 1.5 L/min and Isoflurane dose of 5%. After satisfactory anaesthesia, the Isoflurane dose was reduced to 2.5%.

During procedures the animals were placed on a heating pad (Hot Plate 062, Labotect, Göttingen, Germany) to maintain their body temperature. The anaesthesia was maintained throughout the procedure by a nozzle over the nose and mouth of the animal. As a sign of satisfactory anaesthesia before initiating procedures, the animal's contraction reflex was tested by a pinch at the sole of the back foot with a tweezer.

At the endpoint of the experiment, all mice were sacrificed by cervical dislocation while anaesthetized.

3.2.3 Establishment of tumors

A total of $5x10^5$ E0771 tumor cells suspended in 0.15 mL PBS were subcutaneously injected into the 4^{th} mammary fat pads on each side of the animals. The amount of E0771 tumor cells per mL cell suspension was determined using a NucleoCounter.

The NucleoCounter system is composed of a NucleoCassette for fluorescent staining and safe handling, a NucleoCounter instrument for analysis and two buffers that facilitates efficient fluorescent staining of the cells nucleus (Shah et al., 2006). The first buffer is a lysis buffer that lowers the pH and disrupts the plasma membrane, rendering the nuclei susceptible for fluorescent staining. The second buffer is a stabilizing buffer used to raise the pH of the sample mixture to avoid DNA degradation and optimize the staining. In addition, the lysis and the stabilizing buffers dissolve cell aggregates. The NucleoCassette is a loading device for the for the sample mixture into the NucleoCounter. This loading device is a plastic cartridge internally pre-coated with a fluorescent dye, propidium iodine, which stains the cells nuclei. The NucleoCassette loads a defined amount of the sample mixture (50 µL), thereby enabling the mathematical extrapolation of the cell/mL in a cell culture once the sample mixture was quantified. The NucleoCounter is a cell counting device based on the principle of fluorescent microscopy that detects signals from the stained cells nuclei.

The cells were trypsinized into a single cell suspension, and a 200 µL sample was extracted and mixed with 200 µL of lysis buffer (Reagent A100, 910-0003, ChemoMetech, Allerod, Denmark) and 200 µL of stabilizing buffer (Reagent B, 910-0002, ChemoMetech, Allerod, Denmark). A small sample of the mixture were loaded into a NucloCassette (941-0002, ChemoMetech, Allerod, Denmark) and transferred to a NucleoCounter (NC-100™, ChemoMetech, Allerod, Denmark) for quantification analysis. The total amount of cells in the respective cell culture was thereby determined by multiplying the cell count with the dilution factor in the cell sample and the dilution factor in the cell culture, according to Equation (3.1):

$$\text{Total amount of cells} = \text{Counted cells} * \text{Dilution factor in cell sample} * \text{Dilution factor in cell cuture} \quad (3.1)$$

After identifying the amount of E0771 tumor cells/mL, the cells were centrifugation at 900 rpm at 4^{0}C for 4 min (Eppendorf Centrifuge 5810R, Hamburg, Germany). The RPMI-medium was decanted and PBS was added to obtain a cell suspension of 500,000 cells per 0.15 mL, according to Equation (3.2).

$$\text{Amount of PBS} = \text{Total amount of cells} * \frac{0.15\ \text{mL}}{500{,}000\ \text{Cells}} \quad (3.2)$$

The E0771 cells were then injected subcutaneously into the 4^{th} mammary fat pads on each side of the. Each injection contained 500,000 cells in a 0.15 mL suspension with PBS. The mice were anaesthetized during the injections.

3.3 Treatment

3.3.1 Gleevec

The tyrosine kinase inhibitor Gleevec (Imatinib mesylate, ST571, Novartis Pharma AG, Basel, Switzerland) was obtained as a gift from Novartis Pharmaceutical Corporation. The mice were administered Gleevec (100 mg/kg) once per day by gavage throughout the experiment (4 days).

3.4 Measurements and analysis

3.4.1 Measurement of tumor growth

The injected E0771 cell line formed noticeable tumors in the animals after approximately 4-5 days. After 8-10 days the tumors reached appropriate sizes (approximately 150 mm^3) for initiation of the experiments, hereafter called day 1.

The initial size of each tumor was measured (Figure 3.2) externally by the use of a caliper at day 1, the size of the tumors were re-measured to evaluate the tumor growth at day 4. The tumor shape and position was drawn on a schematic mouse to make sure that the measurement was performed in the same orientation at day 4. The tumor volume was measured bidirectional, assuming the tumor had an elliptical shape. Calculations were performed according to Equation (3.3):

$$\text{Tumor volume } (mm^3) = \left(\pi/6\right) * (a^2 * b) \quad (3.3)$$

Where a is the shortest and b is the longest transversal diameter of the tumor.

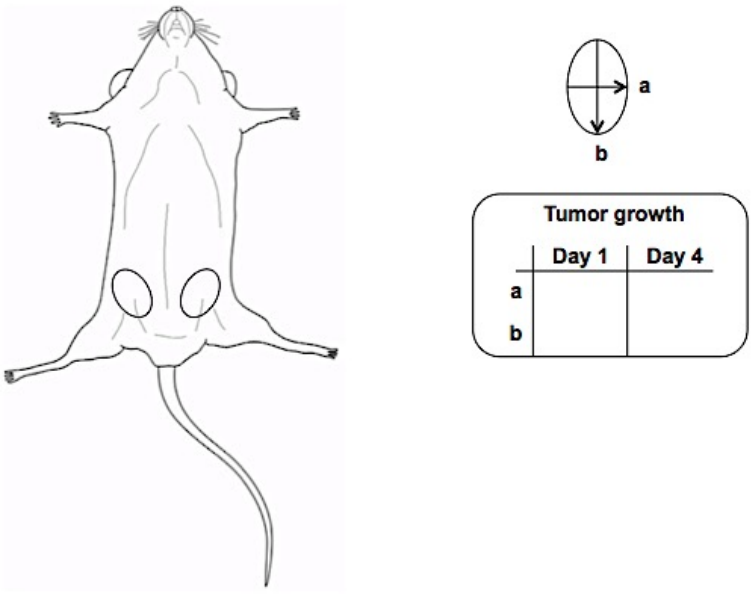

Figure 3.2 Graphical illustration of tumor size measurements.

The Figure illustrates the location and shape of the tumors and the method for tumor size measurements. The letter "a" represents the shortest transversal diameter of the tumor, while the letter "b" represents the longest transversal diameter of the tumor. The Figure is adapted from (Sortland, 2014) with permission.

3.4.2 Measurement of tumor interstitial fluid pressure

The interstitial fluid pressure (IFP) in the tumors was measured using the wick-in-needle technique. In this technique, a fine hypodermic needle (23 Gauge, outer diameter: 0.6 mm) provided with a 2-4 mm long side hole filled with nylon floss (wick) and saline was inserted into the central part of the tumors. Through a PE-50 catheter filled with

saline, the wick-filled needle was connected to a fluid-filled pressure transducer further connected to PowerLab (PowerLab/8sp, ADinstruments Ltd., UK), a high-performance data acquisition system, via an amplifier (Bridge Amp, ADinstruments Ltd., UK). The pressure data was converted to mmHg on a computer using the software Chart5 for windows (PowerLab/8sp ADinstruments Ltd., UK). This setup enabled continuous and stable recordings of the interstitial fluid pressure.

A system calibration was performed before each pressure measurement. In order to calibrate the system, a water column filled to the level of 20 mmHg was connected to the transducer. When the water column exerted pressure of 20 mmHg on the transducer, the electrical output signal was adjusted to 20 mmHg on the computer. The system was thereafter exposed to atmospheric pressure where the electrical output signal was adjusted to 0 mmHg. The system calibrations at 0 mmHg and 20 mmHg provided the software with pressure reference values and enabling accurate pressure measurements.

Before and after each measurement, a zero reference pressure was obtained by placing the needle in a drop of saline at the level of needle insertion site in the tumor. Only measurements with equal (± 1 mmHg) zero pressure reference measurements were accepted.

During each pressure measurement, the fluid communication between the needle and the transducer was confirmed by compression and decompression of the catheter (clamping). The clamping caused a transient rise and fall of the pressure, and only measurements where the pressure returned to the pre-clamped level (± 1 mmHg) was accepted.

IFP measurements were performed earliest 4 hours after the last drug administration. All animals were anaesthetized during for the IFP measurements and placed on a regulated heating pad to keep their body temperature at 38-39^{0}C. After measurements, and while still anaesthetized, the mice were sacrificed by cervical dislocation and the tumors were excised and snap frozen in liquid nitrogen or fixated in 4% formalin (Thermo scientific, Rockford, IL, USA) for further analysis.

3.4.3 Sectioning of frozen tissue samples

The tumor tissue intended for immunohistochemistry were snap frozen in liquid nitrogen after excision and subsequently sectioned into 10 µm sections using a cryostat.

Tissue-Tek (4583, Sakura Finetek Europe B.V, Netherlands) was applied to the specimen disc to connect the frozen tumor tissue to the specimen disc. The tumor tissue was then covered in Tissue-Tek and kept at -21^{o}C until the Tissue-Tek was frozen. The specimen disk was screwed onto the specimen head of the cryostat (Leica CM3050 S Cryostat, Leica Biosystems, Germany) and adjusted so that the knife reached the specimen. The tumor tissue was cut into 10 µm sections and placed onto a SuperFrost plus slide (Thermo Scientific, USA). From each tumor there were made 5 slides with 3-4 tissue sections on each. The slides were stored at -80^{O}C until further use.

3.4.4 Immunohistochemistry staining for CD31

The general principle of immunohistochemistry is the demonstration of antigens within tissue sections by the means of specific antibodies (Ramos-Vara, 2005). CD31, also known as platelet endothelial cell adhesion molecule-1 (PCAM-1) is a 130-kDa membrane-spanning glycoprotein expressed in platelets, monocytes, neutrophils, certain T lymphocytes and vascular endothelial cells (Cicmil et al., 2002). CD31 is involved in angiogenesis, thus the demonstration of its presence by immunohistochemistry is used as a measure of the degree of vascularisation. The protocol used for CD31 immunohistochemistry staining in this thesis was the indirect method, where Rat anti-Mouse CD31 (MCA2388, Bio-Rad, UK) is used as primary antibody and biotinylated Rabbit anti-Rat (PK-4004, Vector Laboratories, Burlingame, CA, USA) is used as secondary antibody.

Frozen tissue sections (10 µm) were fixated in 100-200 µL ice-cold acetone (32201, Sigma-Aldrich, Germany) and stored at -4^{O}C for 10 min. Subsequently, the sections were washed 3 times for 5 min in phosphate buffered saline (PBS) (P3813, Sigma Life Science, USA), pH 7.4. This washing procedure was repeated between each step unless otherwise stated. Any endogenous peroxidase activity was blocked by 30 min incubation in a diluted solution (0.3%) of hydrogen peroxidase (Vnr. 803962, Norges Apotekerforening,

Ås produksjonslab AS) in methanol (322415, Sigma-Aldrich, Germany). Unspecific binding of the primary antibody was blocked by 30 min incubation with rabbit serum (PK-4004, Vector Laboratories, Burlingame, CA, USA) diluted 1:40 in PBS with 0.3% Triton X-100 (PBS-TX) (T8787, Sigma-Aldrich, Germany), pH 7.4. Subsequently, the tissue sections were incubated with the primary antibody Monoclonal Rat anti-Mouse CD31 (clone ER-MP12, MCA2388, Bio-Rad, UK) diluted 1:200 in PBS-TX at $4^{O}C$ overnight.

The following day, the tissue sections were washed with PBS and incubated with the secondary antibody Biotinylated Polyclonal Rabbit anti-Rat IgG (PK-4004, Vector Laboratories, Burlingame, CA, USA) diluted 1:200 in PBS-TX for 30 min. While incubating, the avidin-biotin complex (ABC) solution was prepared (2 drops of Reagent A in 10 mL PBS-TX were mixed followed by addition and mixing of 2 drops of Reagent B) and left in room temperature for 30 min.

After incubation, the tissue sections were washed, first with PBS, then with Tris buffered saline (TBS) (R029, G-Biosciences, St. Louis, MO, USA), pH 7.5. The staining solution 3.3`-Diaminobenzidine (DAB) (ab64238, abcam, Cambridge, UK), which yields a brown color, was then prepared by diluting DAB Chromogen 1:50 in DAB substrate. The tissue sections were incubated with staining solution until desired stain intensity developed (approximately 2-4 min). The staining reaction was quenched by addition of TBS followed by PBS wash.

To achieve a coloration contrast between the tumor tissue and the blood vessels, the tissue sections were counterstained with Richardson stain. Thereby creating a contrast between the tissue, stained in blue with Richardson, and the target antigens, stained in brown with DAB (Figure 3.3).

Counterstaining was performed with Richardson stain followed by washing in ddH_2O to remove excess staining solution. The tissue sections were subsequently dehydrated in increasing concentrations of ethanol (50%, 75%, 96% and 100%) (46139, Sigma-Aldrich, Germany), and xylol (95670, Sigma-Aldrich, Germany). The sections were

mounted with histokitt (1025/500, Glaswarenfabrik Karl Hecht, Germany) and coverslipped.

After staining, all samples were examined using a light microscope (Nikon Eclipse E600, 724064; Nikon, Tokyo, Japan) connected to a camera (Nikon Digital Sight DS-U3, 250430; Nikon, Tokyo, Japan) and a computer with the software NIS Element 3.2 64-bit. The tissue section was examined in a 100x magnification field (i.e., 10x objective lens and 10x ocular lens) to identify microvessel "hot spots" i.e., areas with high concentration of microvessels in the tissue section. Five to seven images were then captured from the hot spots in each tumor at higher magnification (200x). In an organized pattern, the CD31 positive areas were quantified manually per mm^2, and the average number (vessels/mm^2) was calculated. An optical grid was added to each image to enhance quantification.

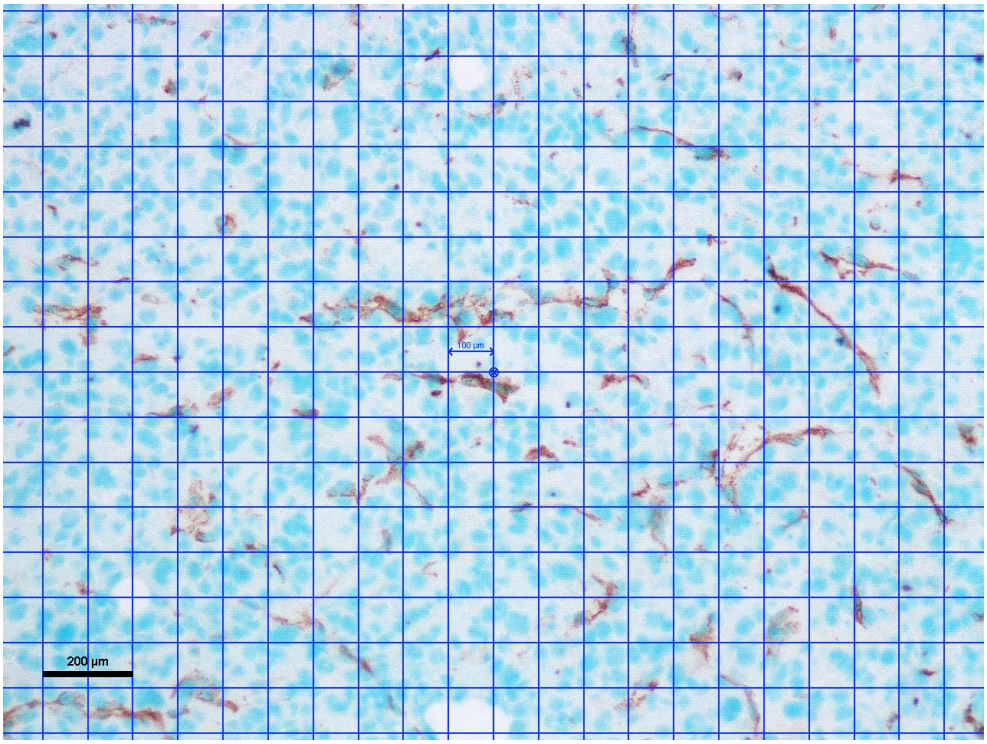

Figure 3.3. Anti-CD31 stained tissue section from an α11-KO mouse.

The Figure displays a representative CD31 stained tissue section from an α11-KO mouse in the Gleevec group. The blood vessels are stained in brown by the staining solution 3.3`-Diaminobenzidine (DAB), while the tissue is counterstained in blue with Richardson stain. The scale bar represents 200 µm. The image was captured at 200x magnification.

3.4.5 Picrosirius red staining

Picrosirius red staining is a commonly used method for visualizing collagen fibrils in paraffin embedded tissue sections. Picrosirius red (F3BA) is a strong, linear anionic dye that can associate along cationic collagen fibres, and enhance their natural birefringence under cross-polarized light (Lattouf et al., 2014). Thus, picrosirius red stained collagen appears red in light microscopy (Figure 3.4).

The tumor tissue intended for picrosirius red staining were fixated in 4% formalin after excision and delivered to the Molecular Imaging Center (Department of Biomedicine, University of Bergen, Norway) for paraffin embedding and sectioning.

The paraffin-embedded tissue sections (4 µm thick) were deparaffinised in xylol (95670, Sigma-Aldrich, Germany) and an ethanol series with decreasing concentration (100%, 96% and 80%)(95670, Sigma-Aldrich, Germany). Followed by hydration under running water for 15 min and incubated with picrosirius red (24901B-250, polysciences, Eppelheim, Germany) staining solution for 60 min. After incubation the tissue section were dehydrated in an ethanol series with increasing concentrations (80%, 96% and 100%) and xylol. The sections were then mounted with histokitt (1025/500, Glaswarenfabrik Karl Hecht, Germany) and coverslipped.

After staining, all samples were examined using a light microscope (Nikon Eclipse E600, 724064; Nikon, Tokyo, Japan) connected to a camera (Nikon Digital Sight DS-U3, 250430; Nikon, Tokyo, Japan) and a computer with the software NIS Element 3.2 64-bit. In an organized pattern, three to five representative images were captured at 200x magnification from each tissue section. The images were analysed with the National Institute of Health ImageJ software, version 1.51s. The collagen density was manually quantified using RGB conversion and the colour threshold tool, the collagen content was quantified based on the picrosirius red positive area (expressed as pixels) of each image, and expressed as the percentage of picrosirius red positive pixels, according to Equation (3.4):

$$\%\ \text{Picrosirius red positive pixels} = \frac{\text{positive area} * 100\%}{(\text{Total area} - \text{deviating area})} \quad (3.4)$$

Where the positive are is the amount of pixels positive for picrosirius red, the total area is the total amount of pixels in the image and the deviating area is the parts (pixels) of the image not suitable for quantification, such as the tumor edge or necrotic tissue.

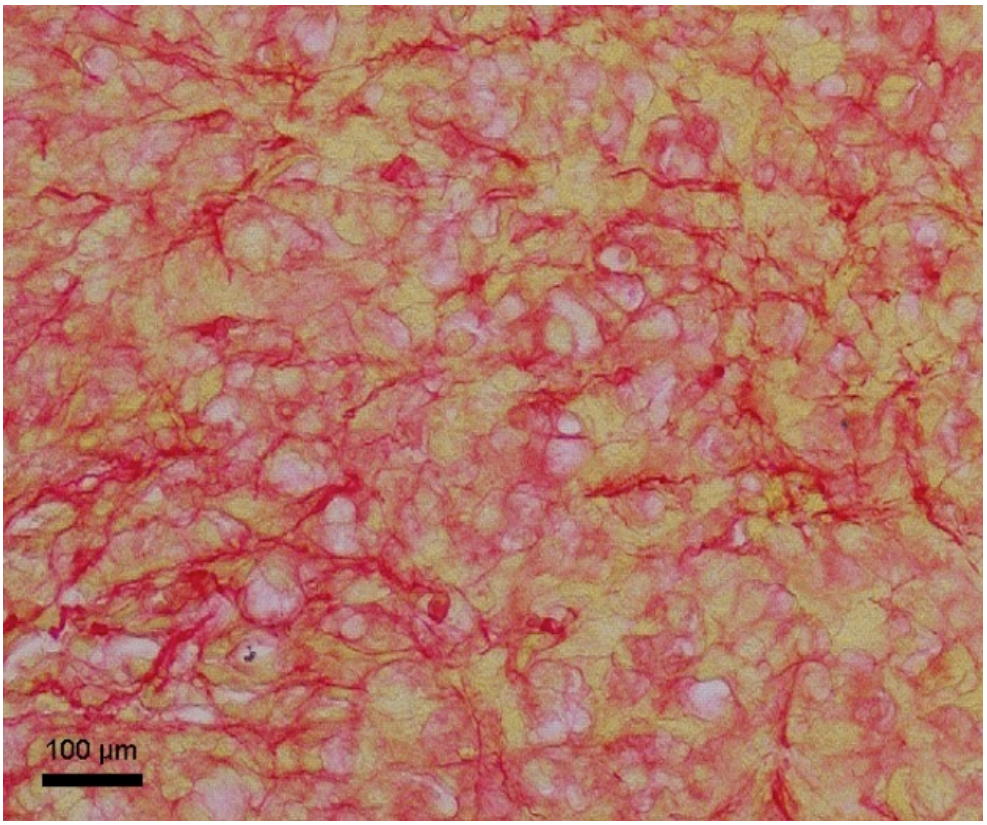

Figure 3.4. Picrosirius red stained tissue section from a WT control mouse.

The Figure displays a representative picrosirius red stained tissue section from a wild type mouse in the control group. The collagen fibrils are shown as red threads. The scale bar represents 100 µm. The image was captured at 200x magnification.

3.4.6 Statistics

Statistical analyses were performed in order to evaluate differences between the groups, and identify the significance of these findings. For statistical analysis, GraphPad Prism 7 (GraphPad Software, Inc., La Jolla, CA, USA) was used. One-way ANOVA with Sidak´s multiple comparisons test was used to analyse statistical differences between the groups. Results were accepted as statistical significant when $p < 0.05$. The data is given as mean ± standard error of mean (SEM) and the number of measurements (n) refers to number of tumors.

4 Results

4.1 Genotyping

The integrin α11 status of all mice used in this thesis was confirmed by genotyping. An earpiece was cut from each mouse and genotyped to verify that they were either α11 KO or α11 WT. Heterozygote mice were used for further breeding to produce α11 KO or α11 WT offspring.

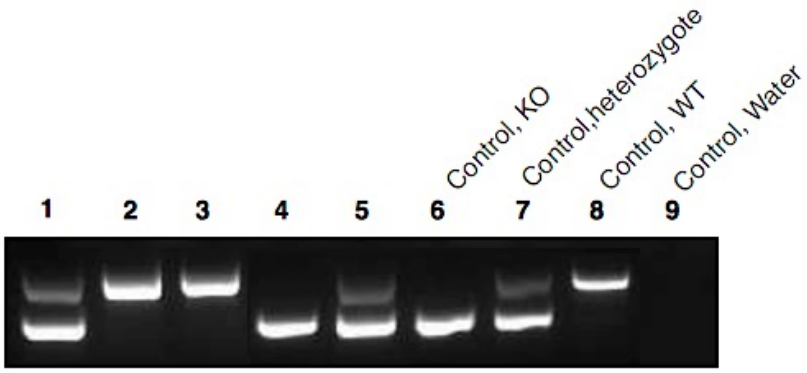

Figure 4.1 Genotyping

The figure displays a representative image of genotyped earpieces from mice in this study. Controls are loaded in well 6-9, containing samples from verified α11 KO, heterozygote (HZ), α11 WT, and water, respectively. Based on the bands from the controls, the samples in well 1-5 are HZ, WT, WT, KO, and HZ, respectively.

4.2 Tumor growth

The size of the E0771 mammary tumors was measured at day 1 and again at day 4 of the experiment, using a caliper. The tumor growth (Figure 4.2) was determined as the average increase in tumor size for all tumors in each group over this four-day period.

The results showed no statistical significant difference in tumor growth between the WT control group and the KO control group, although there is a trend towards a slight reduction in tumor growth in the integrin α11-deficient groups compared WT control.

No significant difference in tumor growth was found between the WT control and the WT Gleevec group either, indicating no effect of Gleevec per se on tumor growth.

Thus, over this four-day period, no influence of integrin α11-deficiency or PDGFR-inhibition on tumor growth was seen. However, the tumor growth was significantly reduced ($p = 0.029$), in the α11-deficient KO control group when compared to the WT Gleevec group, possibly indicating that integrin α11β1 has higher impact on tumor growth than PDGF signalling in these tumor cells.

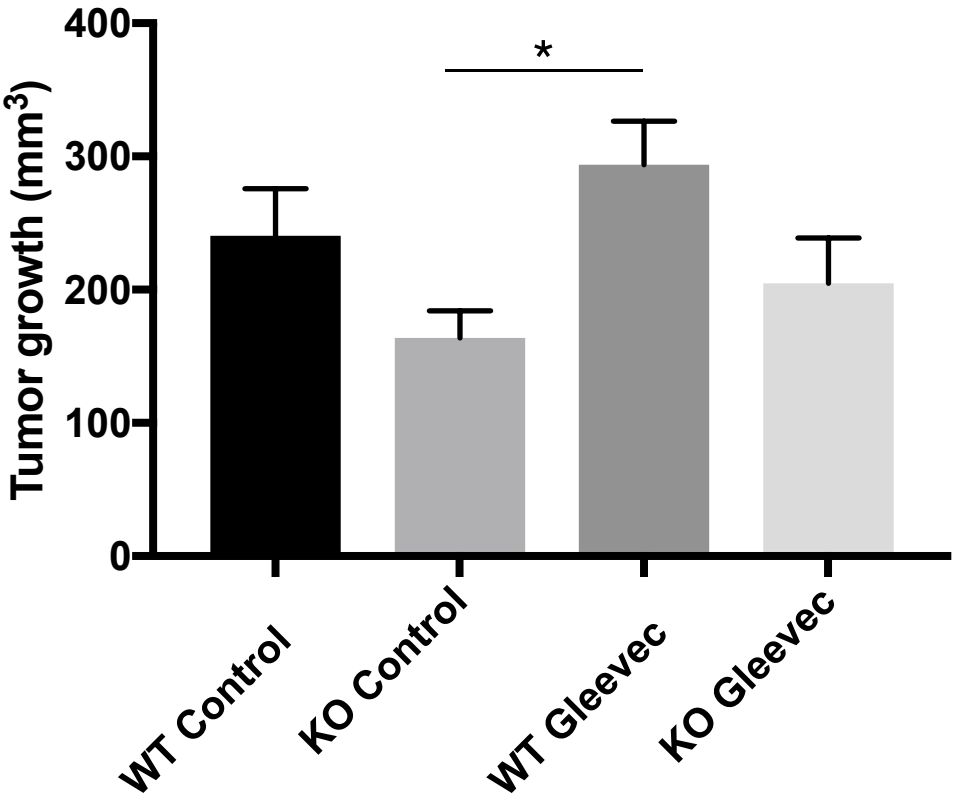

Figure 4.2 Tumor growth.

The columns represent the growth (mm^3) of the E0771 tumors in WT control (n=13), KO control (n=12), WT Gleevec (n=16), and KO Gleevec (n=14) mice. The tumor growth was calculated as the average increase in tumor size for all tumors in each group over a period of four days. The values are given as Means ± SEM. * $p < 0.05$.

4.3 Tumor interstitial fluid pressure

The tumor interstitial fluid pressure (IFP) was determined using the wick-in-needle technique, as described in section 3.4.2. The measurements showed significantly lower IFP in all groups when compared to the WT control group, as shown in Figure 4.3.

The IFP was significantly reduced in the α11-deficient KO control group ($p = 0.002$), the WT Gleevec group ($p = 0.047$) and the KO Gleevec group ($p = 0.013$), suggesting that both integrin α11β1 and PDGF signalling affects IFP to a similar extent in these tumor cells. However, the IFP could not be further supressed by Gleevec in the α11-deficient KO Gleevec group.

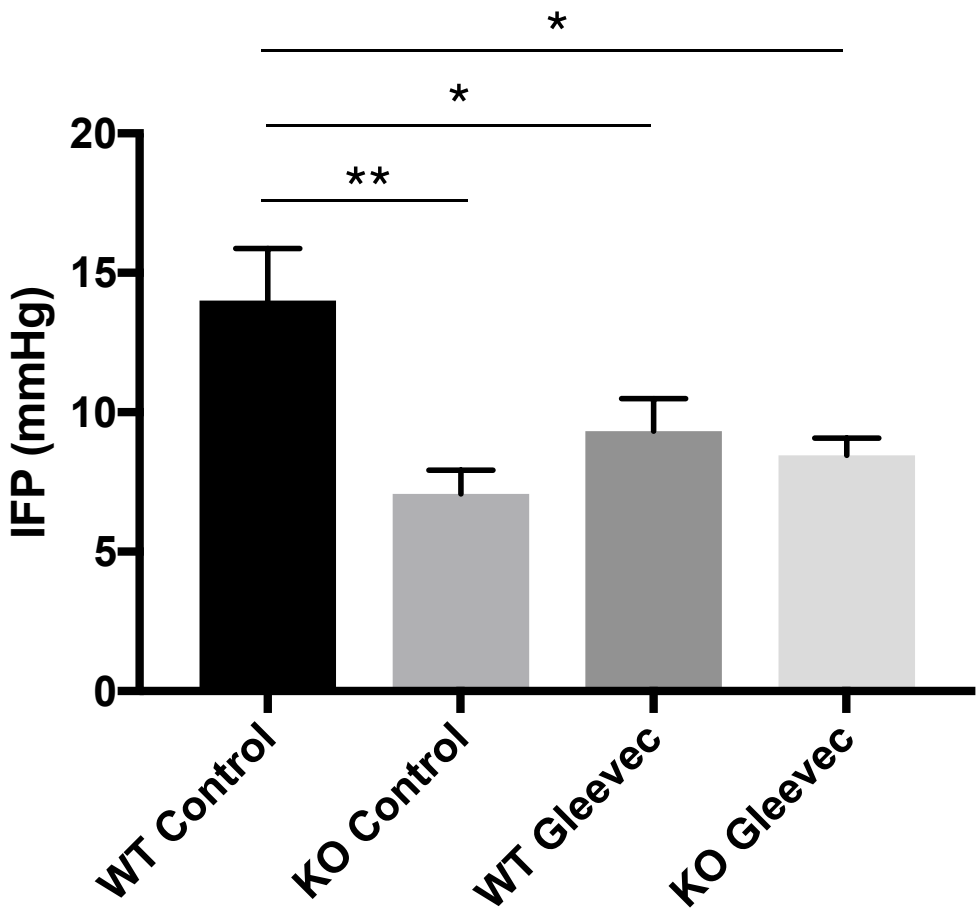

Figure 4.3 Tumor interstitial fluid pressure.

The columns represent the tumor interstitial fluid pressures (mmHg) of the E0771 tumors in WT control (n=13), KO control (n=12), WT Gleevec (n=16), and KO Gleevec (n=14) mice. The tumor IFP was calculated as the average IFP for all tumors in each group. The values are given as Means ± SEM. * $p < 0.05$, ** $p < 0.01$ compared to WT control.

4.4 Tumor blood vessel density

Immunohistochemical anti-CD31 staining was used to quantify the blood vessel density in the tumor tissue sections. For each tumor, five to seven representative images from the viable zone (Figure 4.4) were captured and the amount of blood vessel i.e. the microvessel density (MVD) was manually quantified according to the amount of anti-CD31 stained blood vessels per mm^2, as described in section 3.4.4.

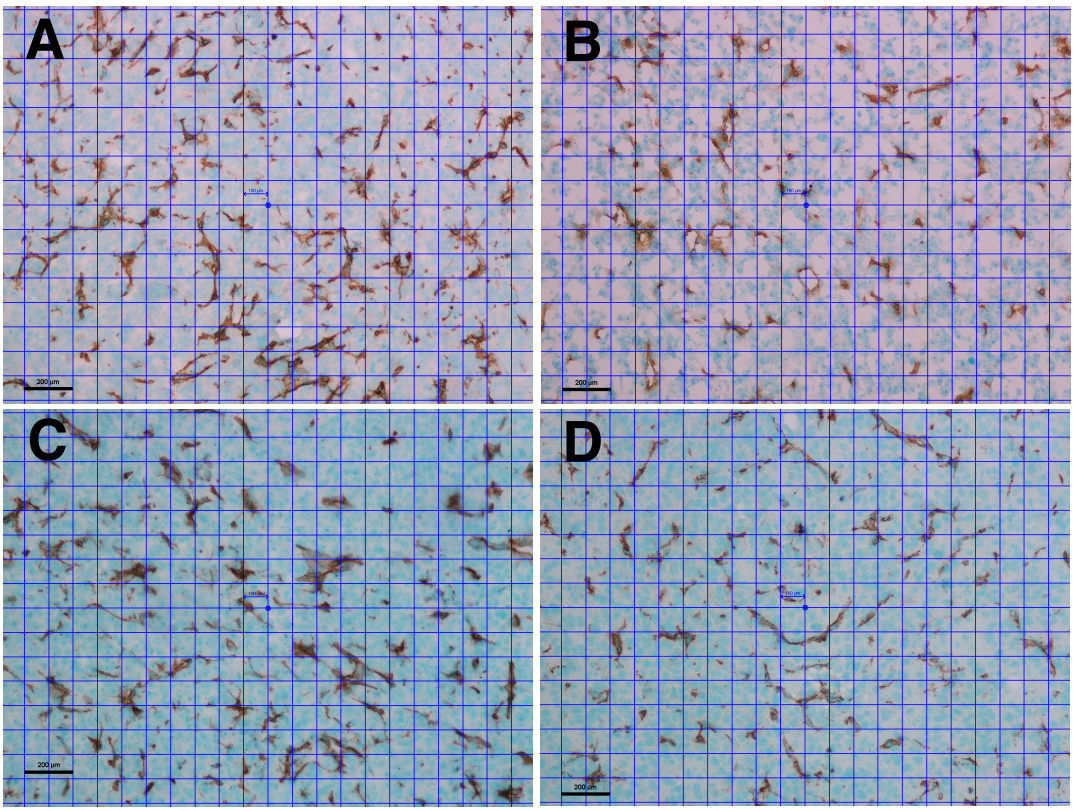

Figure 4.4 Anti-CD31 immunohistochemically stained tissue sections.

The Figure displays representative images from the analysis of tumor blood vessel density in anti-CD31 immunohistochemically stained tissue sections from the WT control group (A), the KO control group (B), the WT Gleevec group (C), and the KO Gleevec group (D). The blood vessels are stained in brown by the staining solution 3.3`-Diaminobenzidine (DAB), while the tissue is counterstained in blue with Richardson stain. The scale bar on the optical grid in the centre of the images indicates grid size of 100 µm, and the scale bar in the lower left hand corner in each image indicates 200 µm. The images were captured at 200x magnification.

The quantification of the anti-CD31 staining showed significant reductions ($p < 0.0001$) in the MVD in all groups when compared to the WT control group, as shown in Figure 4.5. However, the α11-deficient KO control group had significantly lower MVD ($p < 0.0001$) compared to the Gleevec groups (WT Gleevec and KO Gleevec). This may indicating that angiogenesis is more dependent on integrin α11β1 than PDGF signalling in these tumor cells. Furthermore, the results also indicate that the inhibitory effect seen in the α11-deficient KO control group is partially lost in the α11-deficient KO Gleevec group.

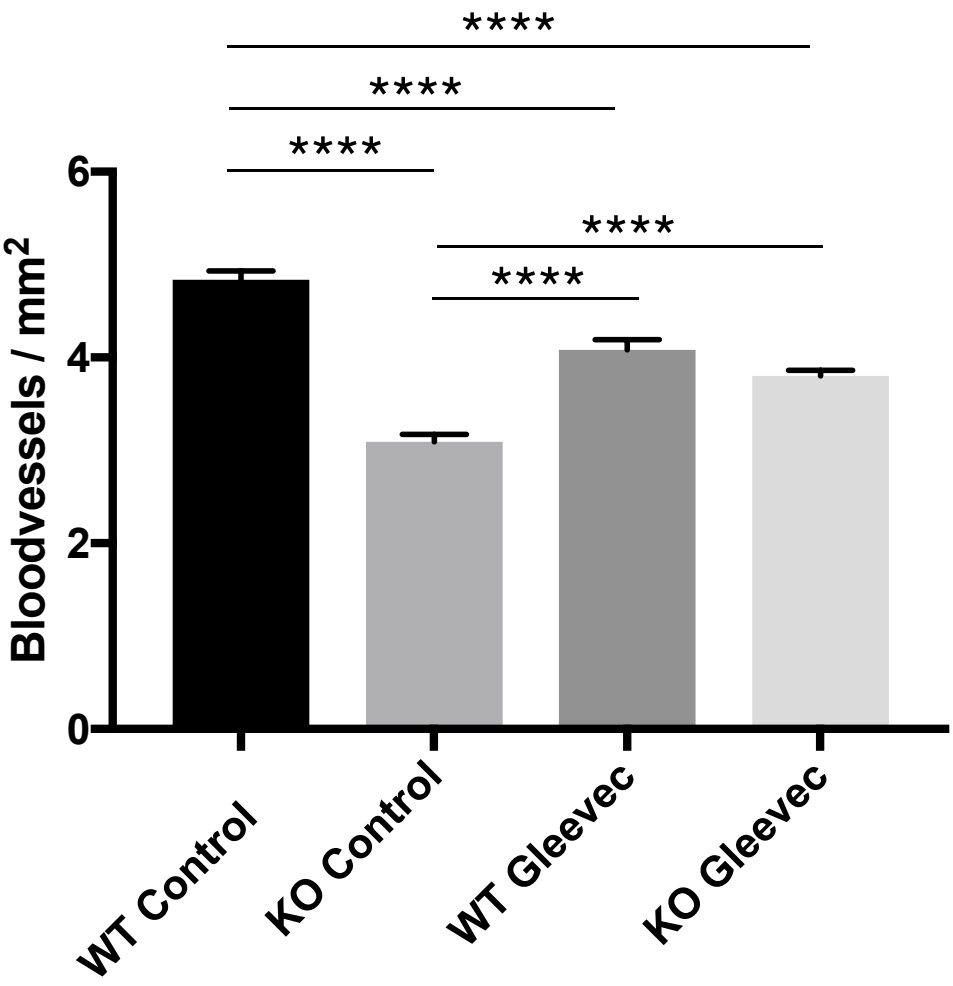

Figure 4.5 Tumor blood vessel density.

The columns represent the tumor blood vessel densities (blood vessel density / mm^2) in tissue sections from WT control (n=6), KO control (n=6), WT Gleevec (n=5), and KO Gleevec (n=6) mice. The tumor blood vessel density was calculated as the average for all tumors sections in each group. The values are given as Means ± SEM. **** $p < 0.0001$.

4.5 Tumor collagen density

Picrosirius-red staining was used to quantify the most abundant collagens, type I and type III, in the tumor sections. For each tumor, three to five representative images (Figure 4.6) were captured to evaluate the tumor collagen density.

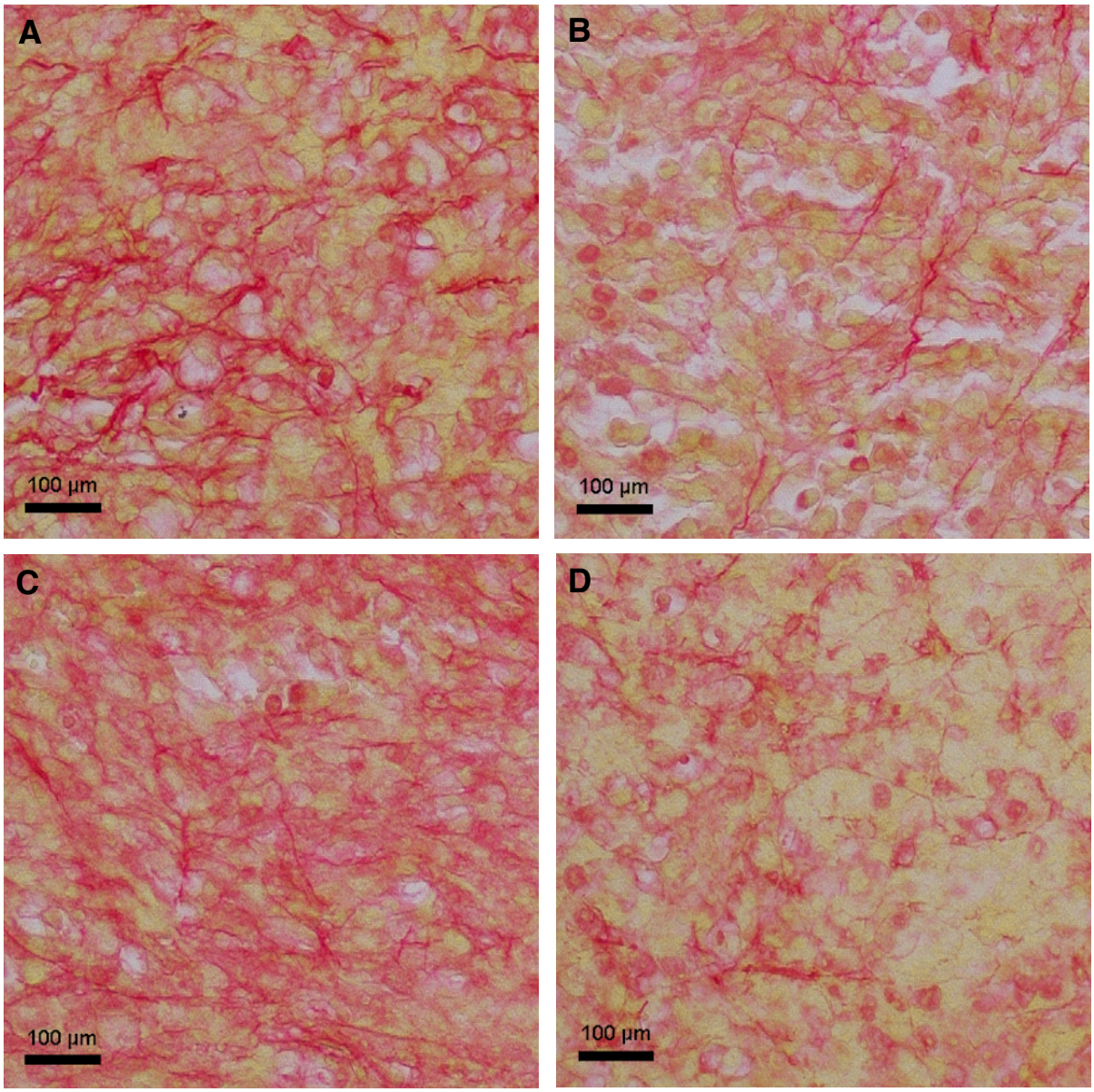

Figure 4.6 Picrosirius red stained tissue sections.

The Figure displays representative images from the analysis of tumor collagen density in picrosirius red stained tissue sections from the WT control group (A), the KO control group (B), the WT Gleevec group (C), and the KO Gleevec group (D). The scale bar in the lower left hand corner in each image indicates 100 µm. The images were captured at 200x magnification.

The collagen density was determined using the ImageJ software and quantified according Equation (3.4), as described in section 3.4.5. The collagen quantification showed (Figure 4.7) a significant reduction in tumor collagen density in the KO control group ($p < 0.0001$), when compared to the WT control group.

No significant difference in collagen density was observed in the WT Gleevec group when compared to the WT control group, or in the α11-deficient KO Gleevec group when compared to the KO control group. Suggesting that the PDGFR-inhibitor Gleevec had no significant effect on the tumor collagen density in these tumors.

The collagen density in the α11-deficient groups, KO control ($p = 0.0002$) and KO Gleevec ($p < 0.0001$), was also found to be significantly lower when compared to the WT Gleevec group. Indicating the importance of integrin $\alpha 11\beta 1$ on the tumor collagen density.

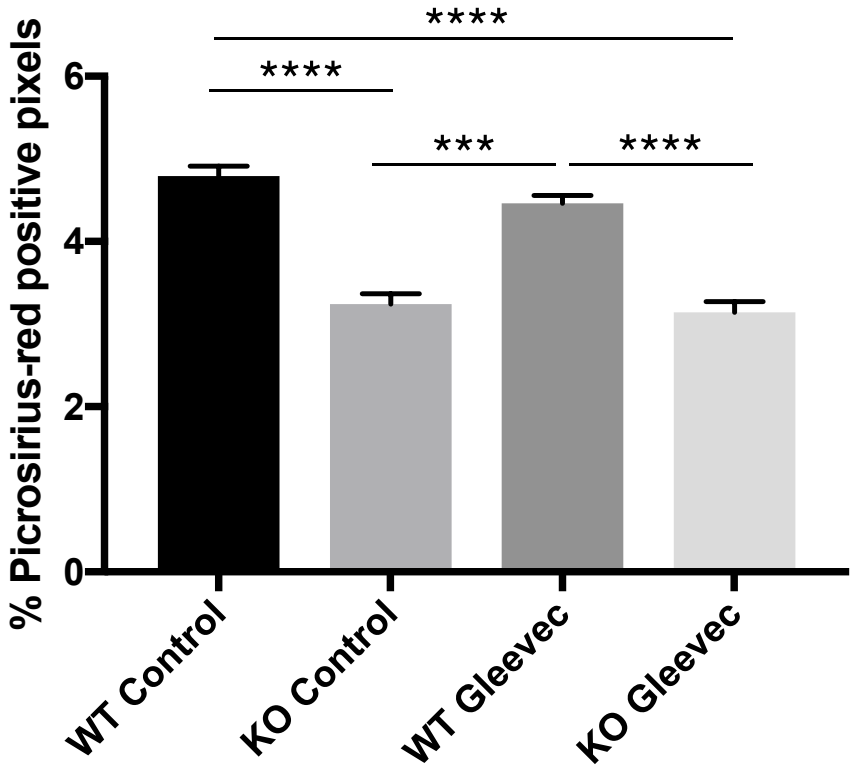

Figure 4.7 Tumor collagen density.

The columns represent the tumor collagen density (% picrosirius-red positive pixels) in WT control (n=4), KO control (n=3), WT Gleevec (n=4), and KO Gleevec (n=4) mice. The tumor collagen density was calculated as the average for all tumors sections in each group. The values are given as Means ± SEM. *** $p = 0.0002$ and **** $p < 0.0001$.

5 Discussion

The discussion section is sub-divided into three sections. The first section consists of a discussion of the methodological aspects of this thesis, mainly the strengths and potential weaknesses of the applied methods. The following sections will provide a general discussion of the results and a conclusion.

5.1 Methodological aspects

5.1.1 Cell line and growth conditions

The objectives of this thesis were to study the *in vivo* effect of integrin α11 and PDGFR-inhibition in triple-negative breast cancer, thus the cell line needed to meet certain criteria. First, it needed to be of the TNBC phenotype. Secondly, it needed to have high take rate and readily grow in the α11-KO mouse strain. Lastly, it needed to express receptor tyrosine kinases, such as PDGFR-β.

The murine E0771 breast cancer cell line used in this thesis, is an aggressive cell line with a TNBC phenotype developed on the C57BL/6 background (VanGundy et al., 2014; Johnstone et al., 2015). These cells readily induce tumors in mice on the C57BL/6 background, such as the α11-KO mouse strain used in this thesis (see section 5.1.2). In addition, a previous study conducted in our lab has demonstrated that the receptor tyrosine kinase PDGFR-β is expressed in E0771 tumor cells (Figure 5.1).

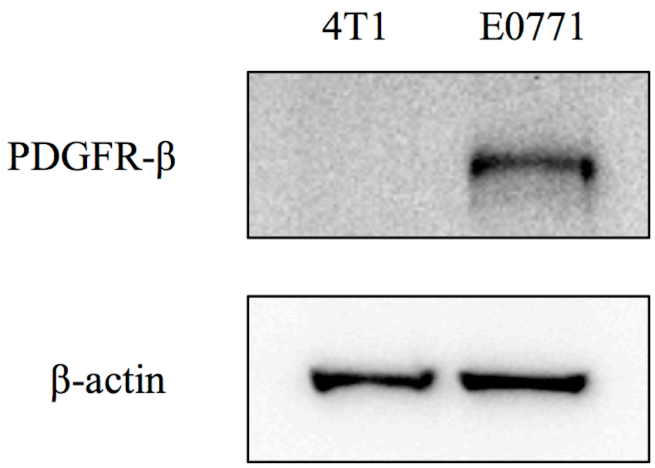

Figure 5.1 PDGFR-β expression in the E0771 murine breast cancer cell line

The western blott depicted in this Figure is a result of a previous study from our lab and demonstrates the expression of PDGFR-β in murine E0771 tumor cells. The expression of PDGFR-β was not found in tumor cells of the TNBC murine cell line 4T1. The Figure was provided by Linda Stuhr.

The E0771 cells were cultured according to the growth conditions recommended by the distributer CH3BioSystems (940001, CH3BioSystems, New York, USA). These growth conditions are also supported by literature (Ewens et al., 2005; Jia et al., 2014).

5.1.2 Animal model

Mice has long served as the preferred animal models in biomedical research due to their anatomical, physiological, and genetic similarity to humans (Bryda, 2013). After the human genome was sequenced in 2001, the mouse genome followed in 2002. Thus, providing a wealth of genetic information on the species. The use of mice for research purposes also has other advantages, the small size and generally mild temperament makes them easy to handle, house and maintain. In addition, mice breed efficiently with short gestation time and relatively large numbers of offspring. Mice also have a fairly rapid development to adulthood.

In this thesis, the integrin α11-deficient heterozygous BALB/c SCID strain was used. This mouse strain is derived from the C57BL/6 strain, which enhances the take rate and

induction of disease with the C57BL/6 derived E0771 cell line (VanGundy et al., 2014; Navab et al., 2016). The mice were bred heterozygously, and the integrin α11 wild type and integrin α11-deficient offspring were used in the experiments. All animal breeding was organized and performed by the technical staff at the animal facility at the Department of Biomedicine, University of Bergen, Norway. All mice used in this study were genotyped and verified as α11 WT or α11 KO by polymerase chain reaction.

5.1.3 Anaesthesia

The animals were subjected to anaesthesia to provide a minimum of stress and pain during the experimental procedures. The method of anaesthesia in this thesis was gas-anaesthesia, using isoflurane in conjunction with oxygen and nitrous oxide.

Isoflurane is the most commonly used volatile anaesthetic for experimental interventions in mice, due to several advantages (Constantinides and Murphy, 2016). Both the induction and recovery time from isoflurane proceeds quickly, within 1-2 min (Cesarovic et al., 2010). The reason for isofluranes rapid induction and recovery times, is explained by its blood/gas partition coefficient, i.e. its solubility in the blood (Dohoo, 1990; Sawyer, 2008, pp. 156-164). The blood/gas partition coefficient describes the relative affinity of an inhalation anaesthetic for the fluid (blood) phase and the gas (alveolar) phase. Isoflurane has a blood/gas partition coefficient of 1.4 at 37^0C, meaning that at equilibrium the concentration of isoflurane in the blood is 1.4 times of the concentration in the gas phase. Inhalation anaesthetics with relatively low solubility in the blood, such as isoflurane, will quickly increase the alveolar concentrations and cause rapid anaesthetic induction, and recovery through pulmonary ventilation (Sawyer, 2008, pp. 156-164).

Another factor that contribute to isofluranes rapid uptake into and elimination from the body, is its high vapour pressure (239.5 mmHg at 20^0C) (Dohoo, 1990). A high vapour pressure means that anaesthetizing concentrations can be rapidly attained, thus decreasing the time for anaesthetic induction. However, this also means that fatal

concentrations may be rapidly attained as well, thus care has to be taken during the anaesthetic procedure.

Isoflurane is a potent cerebral, coronary and peripheral vascular vasodilator (Constantinides and Murphy, 2016). However, N_2O acts as a balancing agent by antagonizing isoflurane-induced vascular vasodilatory responses and thus stabilizing the physiological status of the mice (Constantinides et al., 2011). In fact, the supplemental use of N_2O with isoflurane is associated with higher and more stable values of mean arterial pressure (MAP) and heart rate, including their beat-to-beat variability (Constantinides and Murphy, 2016).

The core body temperature falls during any kind of anaesthesia (Cesarovic et al., 2010). However, due to the small size and high body surface area of mice, they are especially sensitive to hypothermia. As thermoregulation is vital for maintenance of homeostasis in mice, a hot plate set at $37^{O}C$ was used to maintain optimal body temperature during experimental procedures.

5.1.4 Tumor growth

In this thesis, tumor size was measured externally using a caliper. The measurements were collected along the longest two dimensions of the tumor x/y plane and the z-axis dimension was assumed equal to the shortest dimension. The tumor volume was calculated with the assumption of elliptical shape according to Equation 3.3 (Tumor volume = $\pi/6 \times a^2 \times b$), where "a" represents the shortest transversal diameter and "b" represents the longest transversal diameter. The tumor growth was calculated as the post-treatment tumor volume minus the pre-treatment tumor volume.

Measurements of xenograft tumors with calipers are rapid, non-invasive and inexpensive. However, caliper measurements are affected by contributions from epidermis, adipose tissue and fur, each of which introduces error and variability into the volume determination (Ayers et al., 2010). In order to reduce these errors to a minimum, the fur surrounding the tumors were shaved off and the tumor shape was

drawn to obtain measurements in the exact same orientation for both measurement days (day 1 and 4). Each tumor was also measure by the same person, as the intra-individual variability during measurements was assumed to be less then the inter-individual difference. In addition, all animals were anaesthetized during tumor measurements to improve quality of the measurements as well as alleviating the animals of unnecessary stress and discomfort.

There are a number of methods in which more precise measurements of xenograft tumors may be obtained, such as computed tomography (CT), magnetic resonance imaging (MRI) and bioluminescence imaging (BLI). However, these methods are both time consuming and expensive (Ayers et al., 2010). Ultrasound on the other hand, is an inexpensive and non-invasive method for measuring xenograft tumor volume. In a study by Ayers and colleagues in 2010 (Ayers et al., 2010), they compared the accuracy of volume measurements on xenograft tumors using ultrasound imaging and external caliper. Ayers and colleagues found that caliper volume variance was 1.3-fold higher then with ultrasound. Concluding that ultrasound imaging more accurately, and reproducibly reflected the true tumor volume. However, ultrasound imaging requires time-consuming training and was not available at the institute, and therefore not considered as an option in this project.

5.1.5 Tumor interstitial fluid pressure

The measurements of the tumor interstitial fluid pressure were conducted using the well-established wick-in-needle (WIN) technique, as described in section 3.4.2. The WIN technique was developed by Fadnes and colleagues in the late 1970s (Fadnes et al., 1977), in an attempt to combine desirable features from the needle method and the wick catheter technique (Wiig et al., 1986). The WIN technique combines the large contact area from the wick catheter technique with the reasonably atraumatic insertion approach of the needle method, using a thin hypodermic needle (Wiig et al., 1986; Pusenjak and Miklavcic, 1997). Through the combination of these features and fulfilment of the criteria described in section 3.4.2, the WIN technique offers a simple

and convenient way to procure reliable and reproducible IFP measurements in experimentally induced tumors in animals (Wiig and Swartz, 2012).

5.1.6 Immunohistochemistry

Immunohistochemistry is a widely used method to visualise the distribution and amount of certain molecules in tissue by the means of specific antigen-antibody reactions (Kim et al., 2016). In this thesis, immunohistochemistry was used to determine the degree of angiogenesis in the tissue sections, a commonly used surrogate marker of angiogenesis is the MVD, i.e. the number of vessels counted in a given area of tissue (Goddard et al., 2001). In order to visualize and quantify the MVD, tumor sections was immunohistochemically stained for the pan-endothelial marker CD31 (Marien et al., 2016).

5.1.6.1 Immunohistochemical procedure

The immunohistochemical anti-CD31 staining technique used in this thesis was the indirect method. This method can be divided into four main steps. *Step 1* includes all pre-immunologic procedures, such as fixation, blocking endogenous activities and blocking nonspecific bindings (Ramos-Vara et al., 2008). *Step 2* includes all immunologic reactions between the primary antibody and the tissue antigens, the reactions between the primary and the secondary antibody, and the necessary chemical reactions to bind the reporter molecules. *Step 3* includes all procedures necessary for visualization of the antigen-antibody binding. *Step 4* includes the analysis of the results.

Step 1. Pre-immunologic procedures.

The tissue sections were fixated in ice-cold acetone. This type of fixation is known as coagulative fixation (Ramos-Vara et al., 2008). Acetone dehydrates the tissue sections. By removing and replacing free water, acetone destabilizes hydrophobic and hydrophilic interactions. This disrupts the proteins tertiary structure and alters their physical properties, which causes proteins that normally are soluble in aqueous solutions to become insoluble. In this way coagulative fixation maintains the tissue structure and prevents antigen diffusion.

Endogenous peroxidase activity can react with the staining solution DAB to produce a brown product, which is indistinguishable from the specific immunostaining (Ramos-Vara, 2005). This was avoided by pre-treatment of the tissue sections with a diluted solution of hydrogen peroxidase in methanol.

Protein blocking may reduce unwanted background staining, although antibodies have high affinity for the specific target antigen, partial or weak binding to non-specific sites on non-antigen proteins may occur (Kim et al., 2016; thermofisher.com, 2018). This nonspecific binding may cause high background staining that can interfere with the detection of the target antigen.

Step 2. Immunologic procedures.

The indirect immunochemistry method is often referred to as the two-step indirect method, as it consists of two separate layers of antibodies. The first layer is usually a highly specific unlabelled monoclonal antibody for the target antigen (Ramos-Vara, 2005). The second layer is usually a labelled polyclonal antibody that is raised against the primary antibody. This method was developed by Coons and colleagues (Coons et al., 1955) in order to meet the increasing demand for a more sensitive method.

As mentioned, antibodies can either be monoclonal or polyclonal. Monoclonal antibodies are obtained from a single clone of hybridoma, which produce antibodies (Kim et al., 2016). Monoclonal antibodies are highly specific and only bind to a single epitope on an antigen. However, the possibility of cross-reactions with other antigens is not eliminated, as the amino acid sequence of the target epitope may exist in other proteins (Ramos-Vara and Miller, 2014). Polyclonal antibodies are obtained from experimental animals through repetitive stimulations of antigen (Kim et al., 2016). These antibodies are less specific then the monoclonal antibodies and has affinity for a broader range of antigens, which may cause greater nonspecific background staining (Ramos-Vara et al., 2008). Polyclonal antibodies may also affect the reproducibility due to batch variability (Kim et al., 2016).

Both the primary and the secondary antibody used in this thesis are well-known antibodies with high quality literature evidence. In addition, our lab has experience with

the use of these particular antibodies in mice and has established a working protocol for their use in immunohistochemical anti-CD31 staining.

The detection of the immune reaction mostly depends on the detection system. This system needs to have high sensitivity and accuracy, be reproducible and render a high signal-to-noise ratio (Ramos-Vara and Miller, 2014). The ABC method is one of the most common avidin-biotin methods. In this method, HRP conjugated biotin is utilized as the reporter molecule and avidin as a linker, connecting the HRP conjugated biotin to the biotinylated secondary antibody. Avidin is a glycoprotein composed of four identical subunits, each with a binding site for biotin, thereby capable of binding several reporter molecules to each biotinylated antibody (Ramos-Vara, 2005). However, avidin may produce high background by binding lectins or negatively charged tissue components through its carbohydrate groups or through electrostatic interactions due to its high isoelectric point (pI ~ 10).

Step 3. Visualization.

The visualization of the antigens was enabled by addition of DAB, a common staining agent in immunohistochemistry. The enzyme HRP oxidizes and converts DAB to an insoluble polymer, which precipitates as a dark brown pigment at the reaction sites allowing visualization of the target antigens (Dölle et al., 2018).

In order to reduce visual misinterpretations of the immunologic reaction, the tissue sections were counterstained with Richardson´s stain. This staining method produces a blue colour, which eases the visual differentiation of the target antigens in the tissue sections.

Step 4. Analysis.

The intratumoral microvessel density was determined manually using the variant of Weidner approach (Weidner et al., 1991). The tissue section was first scanned using a light microscope at low magnification to identify the areas with the highest microvessel density (the vascular hot spots) in the tumor periphery. Five to ten of these vascular hot spots were selected from each tumor. The microvessels were manually counted under higher magnification (200x), as described in section 3.4.4. An optical grid (100 μm) was

used to aid and enhance counting. Any brown-stained endothelial cell or endothelial-cell cluster that was clearly separated from adjacent microvessel, tumor cells, and other connective-tissue elements was considered a single, countable microvessel (Weidner et al., 1991). Branching vessel structures were counted as a single vessel (Sener et al., 2016). Vascularity was not considered in necrotic areas of the tumor.

The Weidner approach is the most widely used and quoted method for quantification of microvessel density (Goddard et al., 2001; Uzzan et al., 2004). The quantification of microvessels in vascular hot spots is thought to correlate best with the clinical outcome due to its relationship with haematogenous spread (Goddard et al., 2001). The vascular hot spots in the tumor periphery were chosen as these areas are composed of typical capillaries with endothelial cells, derived from pre-existing vessels (Nico et al., 2008). The central areas of the tumor are composed of tube-like endothelial structures and pseudo-vascular channels lined by tumor cells, not endothelial cells (Nico et al., 2008).

5.1.7 Picrosirius red staining

Picrosirius red staining is a common and well-described method for visualization of collagen in tissue sections (Vogel et al., 2015). Sirius red is an elongated molecule containing six salt-forming sulfonic groups, which reacts with the basic amino groups of lysine and hydroxylysine, and the guanidine group of arginine, all of which are found in collagens (Bhutda et al., 2017). Thus, picrosirius red binds to a wide variety of molecules, not just collagens (Rittié, 2017, pp. 395-407). However, the parallel orientation of the picrosirius red molecules along collagen fibrils greatly enhances the natural birefringence of this dye, creating a complex that is much more birefringent than the non-specific complexes between picrosirius red and other proteins. To this effect, picrosirius red-bound fibrillar collagens appear bright and red under polarized light, while the rest of the tissue remains dark (Vogel et al., 2015; Rittié, 2017, pp. 395-407).

The software ImageJ was used to identify the amount of pixels positive for picrosirius red staining. The threshold values were adjusted for each individual image to adjust for differences in intensity and background. The adjustment of threshold values may vary from person to person and thus affect the quantification. To reduce this error source to a

minimum, the same person conducted the threshold adjustment and quantification of all images.

5.2 Discussion of results

5.2.1 Tumor growth

The present study showed no significant reduction in growth of the mammary E0771 tumors in any groups, when compared to the WT control group. However, there is a trend towards a slight reduction in tumor growth in both of the integrin α11-deficient groups, KO control and KO Gleevec. This trend was more pronounced in the KO control group, which also demonstrated a significantly reduction tumor growth compared to the WT Gleevec group.

Similar to these results, Reigstad and colleagues found that integrin α11-deficiency did not affect the growth of murine TNBC cell line 4T1 *in vivo* (Reigstad et al., 2016). However, the same study also showed that integrin α11-deficiency significantly supressed tumor growth in the prostate cancer cell line RM11. In addition, a recent *in vivo* study by Navab and colleagues (Navab et al., 2016) demonstrated that integrin α11-deficiency significantly reduced tumor growth in non-small cell lung carcinoma. Furthermore, a recent *in vivo* study in our group (Hilde Smeland, unpublished data) has demonstrated that integrin α11-deficiency significantly reduces tumor growth in the TNBC cell line MDA-MB-231. The same study also found a trend towards reduced growth in the TNBC cell line MDA-MB-468 (p=0.0568).

Furthermore, using a 3D-heterospheroid model composed of mouse embryonic fibroblasts (α11 WT and α11-KO) and A549 lung carcinoma cells, Lu and colleagues (Lu et al., 2014) found that integrin α11-deficiency resulted in significantly larger tumors. However, the α11-deficient A549 spheroids were less compact then the controls, with significantly reduced tumor cell proliferation.

In the present study, the growth of the E0771 tumors was not significantly affected by Gleevec, neither the WT nor the α11-deficient Gleevec group was found to reduce the tumor growth significantly.

In accordance with these results, no significant *in vivo* effect on tumor growth has been reported for Gleevec in the KAT-4 colonic carcinoma model (Pietras et al., 2002) and in L3.6pl human pancreatic adenocarcinoma (Hwang et al., 2003).

However, Gleevec has been reported to exert a significant inhibitory effect on the proliferation of breast cancer cells *in vitro* (Roussidis et al., 2004; Malavaki et al., 2013; Kadivar et al., 2017). In addition, Blanchard and colleagues (Blanchard et al., 2014) demonstrated that Gleevec significantly reduce the growth of the TNBC cell line MDA-MB-231 *in vivo*. In contrast to these findings, several *in vivo* studies have reported that Gleevec enhanced the growth rate in the TNBC cell lines MA-11 (Rappa et al., 2011) and 4T1 (Samoszuk and Corwin, 2003).

Taken together, these findings suggesting that the effect of both integrin α11-deficiency and Gleevec might be dependent on inter-tumoral differences and/or differences in the specific tumor microenvironments. In addition, this study had a short time frame (four days), it is therefore plausible that larger, and possibly significant, differences in tumor growth might have been found if the time frame was increased.

5.2.2 Tumor interstitial fluid pressure

Elevated interstitial fluid pressure, which is frequently observed in solid tumors, is a result of increased vascular perfusion, impaired lymphatic drainage, high ECM density, and integrin-mediated contraction of interstitial matrix by stromal fibroblasts (Heldin et al., 2004; Stylianopoulos et al., 2018). High vessel permeability increases the outflow of water and solutes into the interstitium, whereas impaired or non-functional lymphatic vessels cause a build-up of interstitial fluid due to ineffective drainage. This is further augmented by a dense and contracted ECM, which resists the percolation of interstitial fluid (Stylianopoulos et al., 2018). High IFP decreases the transcapillary transport in

tumors, and thus impedes the uptake and distribution of anti-cancer therapeutics (Heldin et al., 2004).

In the present study we found that integrin α11-deficiency significantly lowers the tumor IFP, demonstrated by significant reductions in both of the integrin α11-deficient groups compared to the WT control group. In accordance with these findings, our group has recently demonstrated that integrin α11-deficiency significantly lowers the tumor IFP in the TNBC cell lines MDA-MB-231 and MDA-MB-468 *in vivo* (Hilde Smeland, unpublished data). In addition, integrin α11β1 has been demonstrated as a key operator in the maintenance of homeostatic IFP in the dermis *in vivo* (Svendsen et al., 2009; Lidén et al., 2018). Furthermore, using the previously described integrin α11-deficient A549 heterospheroid model, Lu and colleagues (Lu et al., 2014) demonstrated that α11-deficiency significantly reduced the IFP *in vitro.* Taken together, these findings suggest that integrin α11β1 acts as a pressure regulator in solid tumors.

The mechanism in which integrin α11β1 influence the IFP is not completely elucidated. However, integrin α11β1 has been reported as the major collagen-receptor on fibroblasts, regulated by mechanical strain in a transforming growth factor-β (TGF-β)-dependent manner (Carracedo et al., 2010; Schnittert et al., 2018). Integrin α11β1 is involved in the regulation of myofibroblast differentiation, and is thus central to the tumor desmoplasia and ECM contraction (Carracedo et al., 2010). The desmoplastic response results in a stiffer and contracted collagen network which might be more restrictive of changes in the interstitial volume and pose an obstacle for the percolation of interstitial fluid (Heldin et al., 2004; Stylianopoulos et al., 2018). It is therefore plausible that α11-deficiency could impede the effects of myofibroblasts and thereby reduce both the IFP and collagen density in the tumors (see section 5.2.4).

Treatment with the PDGFR-inhibitor Gleevec also resulted in significant reduction of the IFP in the WT Gleevec group. However, no synergistic or additive effect was observed by Gleevec treatment in the α11-deficient KO Gleevec group. In accordance with these results, several *in vivo* studies has demonstrated that Gleevec significantly reduce the

IFP in the colonic carcinoma models CT26 (Burmakin et al., 2017) and KAT-4 (Pietras et al., 2002; Kłosowska-Wardęga et al., 2009; Burmakin et al., 2017).

The mechanism in which Gleevec reduce the IFP is still elusive. However, in an *in vivo* study by Olsson at al., (Olsson et al., 2016) on colorectal KAT-4/HT-29 experimental carcinomas, they found that Gleevec treatment decreased the diameter of the collagen fibrils, resulting in a looser and more flexible collagen network. This disturbance in the collagen ultrastructure allows expansion of the interstitial fluid volume and a subsequent reduction in the IFP. These findings are supportive of our results. We found that Gleevec decreased the IFP, however the collagen density in the E0771 tumor model was unaffected (see section 5.2.4). Indicating that other factors are involved.

5.2.3 Tumor vasculature

Angiogenesis is stimulated growth of new blood vessels from existing vessels, a process that is essential for the progression of cancer (Goddard et al., 2001). Indeed, sustained angiogenesis is one of the hallmarks of cancer and a requirement for tumor growth beyond the initial avascular phase (Hanahan and Weinberg, 2000; Bamias and Dimopoulos, 2003). A commonly used surrogate marker of angiogenesis is the microvessel density (MVD), i.e. the number of vessels counted in a given area of tissue (Goddard et al., 2001). In a meta-analysis conducted by Uzzan and colleagues (Uzzan et al., 2004) high MVD was found as a prognostic factor, significantly predicting poorer survival in women with breast cancer.

In this thesis, we found that integrin α11-deficiency significantly reduced the MVD in both α11-deficient groups compared to the WT control group. Interestingly, the MVD was significantly lower in the α11-deficient control group compared to the α11-deficient Gleevec group. This suggests that inhibition of PDGFR signalling partly repress the anti-angiogenic effect of α11-deficiency in the E0771 tumors. The anti-angiogenic effect of integrin α11-deficiency is largely unexplored, thus the findings in this study might indicate novel roles for integrin $\alpha 11\beta 1$, with the potential for medical applications.

As mentioned, the role of integrin α11β1 in angiogenesis is currently unknown. However, integrin α11β1 is involved in myofibroblast differentiation, as discussed in section 5.2.2 and 5.2.4 (Schnittert et al., 2018). Stromal myofibroblasts are important contributors to tumor angiogenesis and produce a plethora of pro-angiogenic growth factors, including VEGF, TGFβ and PDGFs (Vong and Kalluri, 2011). Furthermore, stromal myofibroblasts are a key source of matrix remodelling proteins, which facilitate and coordinate growing tumor vasculature (Senger and Davis, 2011; Vong and Kalluri, 2011). Thus, the absence of integrin α11β1 might impair the multi-faceted roles of myofibroblasts in tumor progression and angiogenesis.

In the present study, the MVD in both Gleevec groups was significantly reduced compared to the WT control group. In accordance with these findings, Gleevec has been shown to significantly reduce the MVD in the L3.6pl pancreatic adenocarcinoma model (Hwang et al., 2003), A549 non-small cell lung cancer models (Vlahovic et al., 2006, 2007), and in the KAT-4 colonic carcinoma (Kłosowska-Wardęga et al., 2009) *in vivo*.

The PDGF/PDGFR signalling axis has been demonstrated as an important contributor in tumor-associated angiogenesis, and overexpression of PDGFs correlates with increased MVD and poor survival in a range of human cancers (Raica and Cimpean, 2010). PDGFs stimulate endothelial cell proliferation and the secretion of vascular endothelial growth factor (VEGF), a well-described and potent angiogenic inducer (Bamias and Dimopoulos, 2003; Raica and Cimpean, 2010). Particularly, the PDGF-B/PDGFRβ signalling pathway has been shown to play a critical role in the establishment of functional blood vessels through the recruitment and stabilization of perivascular cells (Raica and Cimpean, 2010). Importantly, the coating of perivascular cells, such as pericytes, on the endothelial cells prevents excessive angiogenic sprouting (Cao, 2013). However, PDGF-BB is a potent chemotactic factor for pericytes, thus high levels of tumor cell-derived PDGF-BB may attract pericytes away from blood vessels resulting in decreased pericyte coverage and induction of angiogenesis (Hosaka et al., 2013). This is in accordance with the results found in our study.

5.2.4 Tumor collagen density

Human tumors are stiffer than normal tissue, and this alteration of mechanical properties in tumors reflects increased IFP and compressive loading, ECM stiffening, and elevated cell contractility and rheology (Acerbi et al., 2015). A major contributor to tumor mechanics is the desmoplastic response, which is accompanied by the excessive accumulation of fibrillar collagens, increased remodelling and cross-linking (Acerbi et al., 2015; Kalli and Stylianopoulos, 2018). Desmoplasia and ECM stiffening is characterizing features in many tumor type, and usually promotes tumor progression (Kalli and Stylianopoulos, 2018). In breast cancer, tissue stiffness predicts poor relapse-free survival, reduced therapy response and shorter overall survival (Insua-Rodríguez and Oskarsson, 2016).

In a comprehensive biophysical and histological analysis of human breast tissue, Acerbi and colleagues (Acerbi et al., 2015) demonstrated that breast cancer transformation was accompanied by progressive deposition and remodelling of type I collagen and increased mechanosignalling. The same study also demonstrated that the more aggressive breast cancer subtypes, such as TNBC, was stiffer, more heterogeneous, and contained cells with the higher mechanosignalling compared to less aggressive subtypes.

In the present study we found that the tumor collagen density was significantly lower in the α11-deficient groups compared to both the WT control and the WT Gleevec group, indicating that integrin α11-deficiency impede the excessive accumulation of collagens. This is possibly a result of the involvement of integrin $\alpha 11\beta 1$ in myofibroblast differentiation and desmoplasia.

In contrast to these results, Reigstad and colleagues (Reigstad et al., 2016) found that integrin α11-deficiency did not affect the tumor collagen density in the TNBC cell line 4T1 or the prostate cancer cell line RM11 *in vivo*. Suggesting that the effect of integrin $\alpha 11\beta 1$ on the collagen density may vary between different tumor types.

The receptor tyrosine kinase inhibitor Gleevec did not affect the collagen density. The WT Gleevec group exhibited significantly higher collagen density compared to the α11-deficient groups. Interestingly, the α11-deficient KO Gleevec group had significantly lower collagen density compared to the WT Gleevec group, suggesting that the reduction in collagen density was solely contributed by integrin α11-deficiency.

Consistent with this, a previously described (section 5.2.2) study by Olsson and colleagues (Olsson et al., 2016) reported that Gleevec did not affect the total collagen amount in colorectal KAT-4/HT-29 experimental carcinomas. Instead, Gleevec treatment decreased the diameter of the collagen fibrils, resulting in a looser and more flexible collagen network.

5.3 Conclusion

The main goal of this thesis was to evaluate the *in vivo* effect of integrin α11-deficiency and PDGF-inhibition in the murine E0771 triple-negative breast cancer model. This was addressed through two specific aims:

1. **Evaluate the *in vivo* effect of integrin α11-deficiency on tumor growth, interstitial fluid pressure, angiogenesis, and collagen density in the murine E0771 TNBC model.**

Integrin α11-deficiency did not affect the tumor growth in the murine triple-negative breast cancer E0771 animal model compared to the WT control group. However, the interstitial fluid pressure, microvessel density, and collagen density was significantly reduced in both of the integrin α11-deficient groups. The reduction in interstitial fluid pressure might be caused by reduced collagen density and lower microvessel density. Interestingly, the microvessel density was significantly higher in the KO Gleevec group compared to the KO control group, indicating that α11-deficiency is more efficient in reducing the microvessel density in absence of Gleevec. No synergistic or additive effect was observed in response to inhibition of PDGF signalling in the α11-deficient groups.

2. **Evaluate the *in vivo* effect of PDGF inhibition on tumor growth, interstitial fluid pressure, angiogenesis, and collagen density in the murine E0771 TNBC model.**

The PDGF-inhibitor Gleevec did not affect the tumor growth or the collagen density in the murine E0771 triple-negative breast cancer model compared to the WT control group. The interstitial fluid pressure and microvessel density was significantly reduced in both Gleevec groups compared to the WT control group. However, the WT Gleevec group had significantly higher growth, microvessel density, and collagen density compared to the integrin α11-deficient KO control group. Indicating that PDGF/PDGFR signalling is important in the regulation of pressure homeostasis and angiogenesis in this tumor model.

Taken together, this study indicates that integrin $\alpha 11\beta 1$ promotes a pro-tumorigenic microenvironment. To that effect, integrin $\alpha 11\beta 1$ might represent a novel ECM target for medical applications, especially in adjuvant settings to increase uptake and distribution of systemically administered anti-cancer drugs. However, since the functional roles of integrin $\alpha 11\beta 1$ is not fully uncovered, further investigations are needed to verify these effects in a wider range of tumor types.

The present study also indicated that inhibition of PDGF/PDGFR signalling by Gleevec might increase therapeutic efficiency through the reduction in interstitial fluid pressure and microvessel density. However, further investigations are needed to fully elucidate the mechanism in which the reduction occurs.

6 Future perspectives

The functional roles of integrin α11β1 in the tumor microenvironment are still largely unknown. The findings presented here indicate that integrin α11β1 is an important contributor to a pro-tumorigenic tumor microenvironment in TNBC, impacting the interstitial fluid pressure, microvessel density and collagen density. Considering the influence these factors have on breast cancer progression, integrin α11β1 could potentially represent an attractive target for medical applications, especially in adjuvant settings to increase the efficiency of traditional therapy due to the reduction of IFP. However, the findings presented here should be further investigated to see if they are representative for a wider range of tumor types.

In addition, further investigation on the tumor collagen should be conducted using transmission electron microscopy (TEM) to obtain a wider perspective of how the collagen fibril diameter and organization is affected. In addition, the tumor collagen scaffold architecture should be investigated by scanning electron microscopy (SEM) to evaluate the effects on the tumor collagen network.

Further studies should also investigate the mechanism in which Gleevec reduces the tumor IFP and MVD, and how this is affected by different microenvironments.

7 References

Acerbi, I., Cassereau, L., Dean, I., Shi, Q., Au, A., Park, C., Chen, Y. Y., Liphardt, J., Hwang, E. S. and Weaver, V. M. (2015). Human Breast Cancer Invasion and Aggression Correlates with ECM Stiffness and Immune Cell Infiltration. *Integrative Biology,* 7 (10), pp. 1120–1134.

Alkasalias, T., Moyano-Galceran, L., Arsenian-Henriksson, M. and Lehti, K. (2018). Fibroblasts in the Tumor Microenvironment: Shield or Spear? *International Journal of Molecular Sciences,* 19 (1532), pp. 1–21.

Ayers, G. D., Mckinley, E. T., Zhao, P., Fritz, J. M., Metry, R. E., Deal, B. C., Adlerz, K. M., Coffey, R. J. and Manning, H. C. (2010). Volume of Preclinical Xenograft Tumors Is More Accurately Assessed by Ultrasound Imaging than Manual Caliper Measurements. *Journal of Ultrasound in Medicine,* 29 (6), pp. 891–901.

Bamias, A. and Dimopoulos, A. M. (2003). Angiogenesis in Human Cancer: Implications in Cancer Therapy. *European Journal of Internal Medicine,* 14 (8), pp. 459–469.

Barczyk, M., Carracedo, S. and Gullberg, D. (2010). Integrins. *Cell and Tissue Research,* 339 (1), pp. 269–280.

Baronzio, G., Schwartz, L., Kiselevsky, M., Guais, A., Sanders, E., Milanesi, G., Baronzio, M. and Freitas, I. (2012). Tumor Interstitial Fluid as Modulator of Cancer Inflammation, Thrombosis, Immunity and Angiogenesis. *Anticancer Research,* 32 (2), pp. 405–414.

Baum, J. and Duffy, H. S. (2011). Fibroblasts and Myofibroblasts: What Are We Talking About? *Journal of Cardiovascular Pharmacology,* 57 (4), pp. 376–379.

Bhutda, S., Surve, M., Anil, A., Kamath, K., Singh, N., Modi, D. and Banerjee, A. (2017). Histochemical Staining of Collagen and Identification of Its Subtypes by Picrosirius Red Dye in Mouse Reproductive Tissues. *Bio-Protocol,* 7 (21), pp. 1–10.

Bianchini, G., Balko, J. M., Mayer, I. A., Sanders, M. E. and Gianni, L. (2016). Triple-Negative Breast Cancer: Challenges and Opportunities of a Heterogeneous Disease. *Nature Reviews Clinical Oncology,* 13 (11), pp. 674–690.

Blanchard, Z., Mullins, N., Ellipeddi, P., Lage, J. M., McKinney, S., El-Etriby, R., Zhang, X., Isokpehi, R., Hernandez, B. and ElShamy, W. M. (2014). Geminin Overexpression Promotes Imatinib Sensitive Breast Cancer: A Novel Treatment Approach for Aggressive Breast Cancers, Including a Subset of Triple Negative. *PLoS ONE,* 9 (4), pp. 1–18.

Bray, F., Jemal, A., Grey, N., Ferlay, J. and Forman, D. (2012). Global Cancer Transitions according to the Human Development Index (2008-2030): A Population-Based Study. *The Lancet Oncology,* 13 (8), pp. 790–801.

Bryda, E. C. (2013). The Mighty Mouse: The Impact of Rodents on Advances in Biomedical Research. *Missouri Medicine,* 110 (3), pp. 207–211.

Burmakin, M., Wieringen, T., Olsson, P.O., Stuhr, L., Åhgren, A., Heldin, C. H., Reed,R. K., Rubin, K. and Hellberg, C. (2017). Imatinib Increases Oxygen Delivery in Extracellular Matrix-Rich but Not in Matrix-Poor Experimental Carcinoma. *Journal of Translational Medicine,* 15 (47), pp. 1-9.

Butcher, D. T., Alliston, T. and Weaver, V. M. (2009). A Tense Situation: Forcing Tumour Progression. *Nature Reviews Cancer,* 9 (2), pp. 108–122.

Cao, Y. 2013. "Multifarious Functions of PDGFs and PDGFRs in Tumor Growth and Metastasis." *Trends in Molecular Medicine* 19 (8): 460–473.

Carracedo, S., Lu, N., Popova, S. N., Jonsson, R., Eckes, B. and Gullberg, D. (2010). The Fibroblast Integrin $\alpha 11\beta 1$ Is Induced in a Mechanosensitive Manner Involving Activin A and Regulates Myofibroblast Differentiation. *The Journal of Biological Chemistry,* 285 (14), pp. 10434–10445.

Cesarovic, N., Nicholls, F., Rettich, A., Kronen, P., Hässig, M., Jirkof, P. and Arras, M. (2010). Isoflurane and Sevoflurane Provide Equally Effective Anaesthesia in Laboratory Mice. *Laboratory Animals,* 44 (4), pp. 329–336.

Challapalli, A., Carroll, L. and Aboagye, E. O. (2017). Molecular Mechanisms of Hypoxia in Cancer. *Clinical and Translational Imaging,* 5 (3), pp. 225–253.

Chen, P-H., Chen, X. and He, X. (2013). Platelet-Derived Growth Factors and Their Receptors: Structural and Functional Perspectives. *Biochimica et Biophysica Acta (BBA) - Proteins and Proteomics,* 1834 (10), pp. 2176–2186.

Cho, N. (2016). Molecular Subtypes and Imaging Phenotypes of Breast Cancer. *Ultrasonography,* 35 (4), pp. 281–88.

Cicmil, M., Thomas, J. M., Leduc, M., Bon, C. and Gibbins, J. M. (2002). Platelet Endothelial Cell Adhesion Molecule-1 Signaling Inhibits the Activation of Human Platelets. *Blood,* 99 (1), pp. 137–144.

Collignon, J., Lousberg, L., Schroeder, H. and Jerusalem, G. (2016). Triple-Negative Breast Cancer: Treatment Challenges and Solutions. *Breast Cancer: Targets and Therapy,* 8, pp. 93–107.

Constantinides, C., Mean, R. and Janssen, B. J. (2011). Effects of Isoflurane Anesthesia on the Cardiovascular Function of the C57BL/6 Mouse. *ILAR Journal / National Research Council, Institute of Laboratory Animal Resources,* 52 (3), pp. 21-31.

Constantinides, C. and Murphy, K. (2016). Molecular and Integrative Physiological Effects of Isoflurane Anesthesia: The Paradigm of Cardiovascular Studies in Rodents Using Magnetic Resonance Imaging. *Frontiers in Cardiovascular Medicine,* 3 (23), pp. 1-15

Coons, A. H., Leduc, E. H. and Connolly, J. M. (1955). Studies on Antibody Production I. A Method for the Histochemical Demonstration of Specific Antibody and Its Application to a Study of the Hyperimmune Rabbit. *The Journal of Experimental Medicine,* 102, pp. 49–62.

Cox, T. R. and Erler, J. T. (2011). Remodeling and Homeostasis of the Extracellular Matrix: Implications for Fibrotic Diseases and Cancer. *Disease Models & Mechanisms,* 4, pp. 165–78.

Dohoo, S. E. (1990). Isoflurane Inhalational Anesthetic Agent in Clinical Practice. *The Canadian Veterinary Journal,* 31, pp. 3–6.

Dölle, C., Bindoff, L. A. and Tzoulis, C. (2018). 3,3′-Diaminobenzidine Staining Interferes with PCR-Based DNA Analysis. *Scientific Reports,* 8 (1272), pp. 1–8.

Eroles, P., Bosch, A., Pérez-Fidalgo, J. A. and Lluch, A. (2012). Molecular Biology in Breast Cancer: Intrinsic Subtypes and Signaling Pathways. *Cancer Treatment Reviews,* 38 (6), pp. 698–707.

Ewens, A., Mihich, E. and Ehrke, M. J. (2005). Distant Metastasis from Subcutaneously Grown E0771 Medullary Breast Adenocarcinoma. *Anticancer Research,* 25, pp. 3905–3915.

Exposito, J. Y., Valcourt, U., Cluzel, C. and Lethias, C. (2010). The Fibrillar Collagen Family. *International Journal of Molecular Sciences,* 11 (2), pp. 407–426.

Fadnes, H. O., Reed, R. K. and Aukland, K. (1977). Interstitial Fluid Pressure in Rats Measured with a Modified Wick Technique. *Microvascular Research,* 14 (1), pp. 27–36.

Falke, L. L., Gholizadeh, S., Goldschmeding, R. and Nguyen, T. Q. (2015). Diverse Origins of the Myofibroblast - Implications for Kidney Fibrosis. *Nature Reviews Nephrology,* 11, pp. 233–244.

Farnsworth, R. H., Lackmann, M., Achen, M. G. and Stacker, S. A. (2014). Vascular Remodeling in Cancer. *Oncogene,* 33 (27), pp. 3496–3505.

Ferlay, J., Soerjomataram, I., Dikshit, R., Eser, S., Mathers, C., Rebelo, M., Parkin, D. M., Forman, D. and Bray, F. (2015). Cancer Incidence and Mortality Worldwide: Sources, Methods and Major Patterns in GLOBOCAN 2012. *International Journal of Cancer,* 136 (5), pp. 359–386.

Frantz, C., Stewart, K. M. and Weaver, V. M. (2010). The Extracellular Matrix at a Glance. *Journal of Cell Science,* 123 (24), pp. 4195–4200.

Fulawka, L. and Halon, A. (2017). Ki-67 Evaluation in Breast Cancer: The Daily Diagnostic Practice. *The Indian journal of Pathology and Microbiology,* 60 (2), pp. 177-184.

Gehler, S., Ponik, S. M., Riching, K. M. and Keely, P. J. (2013). Bi-Directional Signaling: Extracellular Matrix and Integrin Regulation of Breast Tumor Progression. *Critical Reviews in Eukaryotic Gene Expression,* 23 (2), pp. 139–157.

Gelse, K., Pöschl, E. and Aigner, T. (2003). Collagens - Structure, Function, and Biosynthesis. *Advanced Drug Delivery Reviews,* 55 (12), pp. 1531–1546.

Geyer, F. C., Pareja, F., Weigelt, B., Rakha, E., Ellis, I. O., Schnitt, S. J. and Reis-Filho, J. S. (2017). The Spectrum of Triple-Negative Breast Disease: High- and Low-Grade Lesions. *The American Journal of Pathology,* 187 (10), pp. 2139–2151.

Goddard, J. C., Sutton, C. D., Berry, D. P., O'Byrne, K. J. and Kockelbergh, R. C. (2001). The Use of Microvessel Density in Assessing Human Urological Tumours. *BJU International,* 87 (9), pp. 866–875.

Goldhirsch, A., Winer, E. P., Coates, A. S., Gelber, R. D., Piccart-Gebhart, M., Thürlimann, B., Senn, H-J. and Panel members. (2013). Personalizing the Treatment of Women with Early Breast Cancer: Highlights of the St Gallen International Expert Consensus on the Primary Therapy of Early Breast Cancer 2013. *Annals of Oncology,* 24 (9), pp. 2206–2223.

Goldhirsch, A., Wood, W. C., Coates, A. S., Gelber, R. D., Thürlimann, B., Senn, H-J. and Panel members. (2011). Strategies for Subtypes — Dealing with the Diversity of Breast Cancer: Highlights of the St Gallen International Expert Consensus on the Primary Therapy of Early Breast Cancer 2011. *Annals of Oncology,* 22, pp. 1736–1747.

Goswami, S. (2013). Importance of Integrin Receptors in the Field of Pharmaceutical & Medical Science. *Advances in Biological Chemistry,* 3 (2), pp. 224–252.

Gullberg, D, Velling, T., Sjoberg, G. and Sejersen, T. (1995). Up-Regulation of a Novel Integrin α-Chain (α_{mt}) on Human Fetal Myotubes. *Developmental Dynamics,* 204, pp. 57–65.

Hamidi, H., Pietila, M. and Ivaska, J. (2016). The Complexity of Integrins in Cancer and New Scopes for Therapeutic Targeting. *British Journal of Cancer* 115, pp. 1017–1023.

Hanahan, D. and Weinberg, R. A. (2000). The Hallmarks of Cancer. *Cell,* 100 (1), pp. 57–70.

Hanahan, D. and Weinberg, R. A. (2011). Hallmarks of Cancer: The Next Generation. *Cell,* 144 (5), pp. 646–74.

Handorf, A. M., Zhou, Y., Halanski, M. A. and Li, W-J. (2015). Tissue Stiffness Dictates Development, Homeostasis, and Disease Progression. *Organogenesis,* 11 (1), pp. 1–15.

Hanley, C. J., Mellone, M., Ford, K., Thirdborough, S. M., Mellows, T., Frampton, S. J., Smith, D. M., Harden, E., Szyndralewiez, C., Bullock, M., Noble, F., Moutasim, K. A., King, E. V., Vijayanand, P., Mirnezami, A. H., Underwood, T. J., Ottensmeier, C. H. and Thomas, G. J. (2018). Targeting the Myofibroblastic Cancer-Associated Fibroblast Phenotype Through Inhibition of NOX4. *Journal of the National Cancer Institute,* 110 (1), pp. 109–120.

Harburger, D. S. and Calderwood, D. A. (2009). Integrin Signalling at a Glance. *Journal of Cell Science* 122, pp. 159–163.

Haslene-Hox, H., Tenstad, O. and Wiig, H. (2013). Interstitial Fluid - A Reflection of the Tumor Cell Microenvironment and Secretome. *Biochimica et Biophysica Acta - Proteins and Proteomics,* 1834 (11), pp. 2336–2346.

Heldin, C-H. and Lennartsson, J. (2013). Structural and Functional Properties of Platelet-Derived Growth Factor and Stem Cell Factor Receptors. *Cold Spring Harbor Perspectives in Biology* 5 (8), pp. 1–19.

Heldin, C-H., Lennartsson, J. and Westermark, B. (2018). Involvement of Platelet-Derived Growth Factor Ligands and Receptors in Tumorigenesis. *Journal of Internal Medicine,* 283 (1), pp. 16–44.

Heldin, C-H. (2013). Targeting the PDGF Signaling Pathway in Tumor Treatment. *Cell Communication and Signaling,* 11 (97), pp. 1–18. doi:10.1186/1478-811X-11-97.

Heldin, C-H. (2014). Targeting the PDGF Signaling Pathway in the Treatment of Non-Malignant Diseases. *Journal of Neuroimmune Pharmacology,* 9 (2), pp. 69–79.

Heldin, C-H., Rubin, K., Pietras, K. and Östman, A. (2004). High Interstitial Fluid Pressure - An Obstacle in Cancer Therapy. *Nature Reviews Cancer,* 4 (10), pp. 806–813.

Hoff, P. M. and Machado, K. K. (2012). Role of Angiogenesis in the Pathogenesis of Cancer. *Cancer Treatment Reviews,* 38 (7), pp. 825–833.

Hosaka, K., Yang, Y., Seki, T., Nakamura, M., Andersson, P., Rouhi, P., Yang, X., Jensen, L., Lim. S., Feng, N., Xue, Y., Li, X., Larsson, O., Ohhashi, T. and Cao, Y. (2013). Tumour PDGF-BB Expression Levels Determine Dual Effects of Anti-PDGF Drugs on Vascular Remodelling and Metastasis. *Nature Communications,* 4 (2129), pp. 1–14.

Humphries, J. D., Byron, A. and Humphries, M. J. (2006). Integrin Ligands at a Glance. *Journal of Cell Science,* 119 (19), pp. 3901–3903.

Hwang, R. F., Yokoi, K., Bucana, C. D., Tsan, R., Killion, J. J., Evans, D. B. and Fidler, I. J. (2003). Inhibition of Platelet-Derived Growth Factor Receptor Phosphorylation by STI571 (Gleevec) Reduces Growth and Metastasis of Human Pancreatic Carcinoma in an Orthotopic Nude Mouse Model. *Clinical Cancer Research,* 9 (713), pp. 6534–6544.

Insua-Rodríguez, J. and Oskarsson, T. (2016). The Extracellular Matrix in Breast Cancer. *Advanced Drug Delivery Reviews,* 97, pp. 41–55.

Iqbal, N. and Iqbal, N. (2014). Imatinib: A Breakthrough of Targeted Therapy in Cancer. *Chemotherapy Research and Practice,* 2014, pp. 1–9.

Jia, X., Yu, F., Wang, J., Iwanowycz, S., Saaoud, F., Wang, Y., Hu, J., Wang, Q. and Fan, D. (2014). Emodin Suppresses Pulmonary Metastasis of Breast Cancer Cells Accompanied with Decreased Macrophage Recruitment and M2 Polarization in the Lungs. *Breast Cancer Research and Treatment,* 148 (2), pp. 291–302.

Johnstone, C. N., Smith, Y. E., Cao, Y., Burrows, A. D., Cross, R. S. N., Ling, X., Redvers, R. P., Doherty, J. P., Eckhardt, B. L., Natoli, A. L., Restall, C. M., Lucas, E., Pearson, H. B., Deb, S., Britt, K. L., Rizzitelli, A., Li, J., Harmey, J. H., Pouliot, N. and Anderson, R. L. (2015). Functional and Molecular Characterisation of EO771.LMB Tumours, a New C57BL/6-Mouse-Derived Model of Spontaneously Metastatic Mammary Cancer. *Disease Models & Mechanisms,* 8 (3), pp. 237–251.

Kadivar, A., Kamalidehghan, B., Javar, H. A., Karimi, B., Sedghi, R. and Noordin, M. I. (2017). Antiproliferation Effect of Imatinib Mesylate on MCF7, T-47D Tumorigenic and Mcf 10A Nontumorigenic Breast Cell Lines via PDGFR-B, PDGF-BB, c-Kit and SCF Genes. *Drug Design, Development and Therapy,* 11, pp. 469–81.

Kalli, M. and Stylianopoulos, T. (2018). Defining the Role of Solid Stress and Matrix Stiffness in Cancer Cell Proliferation and Metastasis. *Frontiers in Oncology,* 8 (55), pp. 1–7.

Kendall, R. T. and Feghali-Bostwick, C. A. (2014). Fibroblasts in Fibrosis: Novel Roles and Mediators. *Frontiers in Pharmacology,* 5 (123), pp. 1–13.

Kim, S-W., Roh, J. and Park, C-S. (2016). Immunohistochemistry for Pathologists: Protocols, Pitfalls, and Tips. *Journal of Pathology and Translational Medicine,* 50 (6), pp. 411–418.

Kim, S. M., Faix, P. H. and Schnitzer, J. E. (2017). Overcoming Key Biological Barriers to Cancer Drug Delivery and Efficacy. *Journal of Controlled Release,* 267, pp. 15–30.

Kłosowska-Wardęga, A., Hasumi, Y., Burmakin, M., Åhgren, A., Stuhr, L., Moen, I., Reed, R. K., Rubin, K., Hellberg, C. and Heldin, C-H. (2009). Combined Anti-Angiogenic Therapy Targeting PDGF and Vegf Receptors Lowers the Interstitial Fluid Pressure in a Murine Experimental Carcinoma. *PLoS ONE,* 4 (12), pp. 1-7

Kreftregisteret.no. (2016). Kreftstatsistikk. [online] https://www.kreftregisteret.no/Registrene/Kreftstatistikk/ [Accessed 29. June 2018].

Lal, S., Reed, A. E. M., de Luca, X. M. and Simpson, P. S. (2017). Molecular Signatures in Breast Cancer. *Methods,* 131 (1), pp. 135–146.

Lattouf, R., Younes, R., Lutomski, D., Naaman, N., Godeau, G., Senni, K. and Changotade, S. (2014). Picrosirius Red Staining: A Useful Tool to Appraise Collagen Networks in Normal and Pathological Tissues. *Journal of Histochemistry and Cytochemistry,* 62 (10), pp. 751–758.

Levental, K. R., Yu, H., Kass, L., Lakins, J. N., Egeblad, M., Erler, J. T., Fong, S. F. T., Csiszar, K., Giaccia, A., Weininger, W., Yamauchi, M., Gasser, D. L. and Weaver, V. M. (2009). Matrix Crosslinking Forces Tumor Progression by Enhancing Integrin Signaling. *Cell,* 139 (5), pp. 891–906.

Levick, J. R. (2010). Circulation of fluid between plasma, interstitium and lymph. In *An introduction to Cardiovascular Physiology*. 5th ed. London: Hodder Arnold, pp. 188-212.

Lidén, Å., Karlsen, T. V., Guss, B., Reed, R. K. and Rubin, K. (2018). Integrin αVβ3 Can Substitute for Collagen-Binding β1-Integrins in Vivo to Maintain a Homeostatic Interstitial Fluid Pressure. *Experimental Physiology,* 103 (5), pp. 629–634.

Logsdon, E. A., Finley, S. D., Popel, A. S. and MacGabhann, F. (2014). A Systems Biology View of Blood Vessel Growth and Remodelling. *Journal of Cellular and Molecular Medicine,* 18 (8), pp. 1491–1508.

Loizzi, V., del Vecchio, V., Gargano, G., de Liso, M., Kardashi, A., Naglieri, E., Resta, L., Cicinelli, E. and Cormio, G. (2017). Biological Pathways Involved in Tumor Angiogenesis and Bevacizumab Based Anti-Angiogenic Therapy with Special References to Ovarian Cancer. *International Journal of Molecular Sciences,* 18 (9), pp. 1–11.

Lu, N., Karlsen, T. V., Reed, R. K., Kusche-Gullberg, M. and Gullberg, D. (2014). Fibroblast α11β1 Integrin Regulates Tensional Homeostasis in fibroblast/A549 Carcinoma Heterospheroids. *PLoS ONE,* 9 (7), pp. 1-13.

Makki, J. (2015). Diversity of Breast Carcinoma: Histological Subtypes and Clinical Relevance. *Clinical Medicine Insights: Pathology,* 8 (1), 23–31.

Malavaki, C. J., Roussidis, A. E., Gialeli, C., Kletsas, D., Tsegenidis, T., Theocharis, A. D., Tzanakakis, G. N. and Karamanos, N. K. (2013). Imatinib as a Key Inhibitor of the Platelet-Derived Growth Factor Receptor Mediated Expression of Cell Surface Heparan Sulfate Proteoglycans and Functional Properties of Breast Cancer Cells. *FEBS Journal,* 280 (10), pp. 2477–2489.

Marien, K. M., Croons, V., Waumans, Y., Sluydts, E., De Schepper, S., Andries, L., Waelput, W., Fransen, E., Vermeulen, P. B., Kockx, M. M. and De Meyer, G. R. Y. (2016). Development and Validation of a Histological Method to Measure Microvessel Density in Whole-Slide Images of Cancer Tissue. *PLoS ONE,* 11 (9), pp. 1–20.

Mas-moruno, C., Rechenmacher, F. and Kessler, H. (2010). Cilengitide: The First Anti-Angiogenic Small Molecule Drug Candidate. Design, Synthesis and Clinical Evaluation. *Anti-Cancer Agents in Medical Chemistry,* 10, pp. 753–768.

Muiznieks, L. D. and Keeley, F. W. (2013). Molecular Assembly and Mechanical Properties of the Extracellular Matrix: A Fibrous Protein Perspective. *BBA - Molecular Basis of Disease,* 1832 (7), pp. 866–875.

Navab, R., Strumpf, D., To, C., Pasko, E., Kim, K. S., Park, C. J., Hai, J., Liu, J., Jonkman, J., Barczyk, M., Bandarchi, B., Wang, Y. H., Venkat, K., Ibrahimov, E., Pham, N-A., Radulovich, N., Zhu, C-Q., Pintilie, M., Wang, D., Lu, A., Jurisica, I., Walker, G. C., Gullberg, D. and Tsao, M-S. (2016). Integrin α11β1 Regulates Cancer Stromal Stiffness and Promotes Tumorigenicity and Metastasis in Non-Small Cell Lung Cancer. *Oncogene,* 35, pp. 1899–1908.

Nbcf. org.au. (2016). Breast Anatomy and How Cancer Starts. [online] https://nbcf.org.au/about-national-breast-cancer-foundation/about-breast-cancer/what-you-need-to-know/breast-anatomy-cancer-starts/ [Accessed 2. July 2018].

Nico, B., Benagiano, V., Mangieri, D., Maruotti, N., Vacca, A. and Ribatti, D. (2008). Evaluation of Microvascular Density in Tumors: Pro and Contra. *Histology and Histopathology,* 23 (5), pp. 601–607.

Nicolini, A., Ferrari, P. and Duffy, M. J. (2018). Prognostic and Predictive Biomarkers in Breast Cancer: Past, Present and Future. *Seminars in Cancer Biology,* 52 (1), pp. 56-73

Northey, J. J., Przybyla, L. and Weaver, V. M. (2017). Tissue Force Programs Cell Fate and Tumor Aggression. *Cancer Discovery,* 7 (11), 1224–1237.

Olsson, P. O., Gustafsson, R., in 't Zandt, R., Friman, T., Maccarana, M., Tykesson, E., Oldberg, Å., Rubin, K. and Kalamajski, S. (2016). The Tyrosine Kinase Inhibitor Imatinib Augments Extracellular Fluid Exchange and Reduces Average Collagen Fibril Diameter in Experimental Carcinoma. *Molecular Cancer Therapeutics,* 15 (10), pp. 2455–2464.

Pecorino, Lauren. (2012). *Molecular Biology of Cancer*. 3rd ed. Oxford: Oxford University Press.

Perou, C. M., Sørlie, T., Eisen, M. B., van de Rijn, M., Jeffrey, S. S., Rees, C. A., Pollack, J. R., Ross, D., Johnsen, H., Akslen, L. A., Fluge, Ø., Pergamenschikov, A., Williams, C., Zhu, S. X., Lønning, P. E., Børresen-Dale, A-L., Brown, P. O. and Botstein, D. (2000). Molecular Portraits of Human Breast Tumours. *Nature,* 406 (6797), pp. 747–752.

Pietras, K., Rubin, K., Sjoblom, T., Buchdunger, E., Sjoquist, M., Heldin, C-H and Ostman, A. (2002). Inhibition of PDGF Receptor Signaling in Tumor Stroma Enhances Antitumor Effect of Chemotherapy. *Cancer Research,* 62, pp. 5476–5484.

Pittman, R. N. (2013). Oxygen Transport in the Microcirculation and Its Regulation. *Microcirculation,* 20 (2), pp. 117–137.

Prat, A., Pineda, E., Adamo, B., Galván, P., Fernández, A., Gaba, L., Díez, M., Viladot, M., Arance, A. and Muñoz, M. (2015). Clinical Implications of the Intrinsic Molecular Subtypes of Breast Cancer. *The Breast,* 24: 26–35.

Pusenjak, J. and Miklavcic, D. (1997). Interstitial Fluid Pressure as an Obstacle in Treatment of Solid Tumors. *Radiology and Oncology,* 31, pp. 291–297.

Raica, M. and Cimpean, A. M. (2010). Platelet-Derived Growth Factor (PDGF)/PDGF Receptors (PDGFR) Axis as Target for Antitumor and Antiangiogenic Therapy. *Pharmaceuticals,* 3 (3), pp. 572–599.

Ramage, L. (2012). Integrins and Extracellular Matrix in Mechanotransduction. *Cell Health and Cytoskeleton,* 4, pp. 1–9.

Ramos-Vara, J. A. (2005). Technical Aspects of Immunohistochemistry. *Veterinary Pathology,* 42 (4), pp. 405–426.

Ramos-Vara, J. A., Kiupel, M., Baszier, T., Bliven, L., Brodersen, B., Chelack, B., Czub, S., Del Piero, F., Dial, S., Ehrhart, E. J., Graham, T., Manning, L., Paulsen, D., Valli, V. E. and West, K. (2008). Suggested Guidelines for Immunohistochemical Techniques in Veterinary Diagnostic Laboratories. *Journal of Veterinary Diagnostic Investigation,* 20 (4), pp. 393–413.

Ramos-Vara, J. A. and Miller, M. A. (2014). When Tissue Antigens and Antibodies Get Along: Revisiting the Technical Aspects of Immunohistochemistry — The Red, Brown, and Blue Technique. *Veterinary Pathology,* 51 (1), pp. 42–87.

Rappa, G., Anzanello, F. and Lorico, A. (2011). Imatinib Mesylate Enhances the Malignant Behavior of Human Breast Carcinoma Cells. *Cancer Chemotherapy and Pharmacology,* 67 (4), pp. 919–926.

Reigstad, I., Smeland, H. Y-H., Skogstrand, T., Sortland, K., Schmid, M. C., Reed, R. K. and Stuhr, L. (2016). Stromal Integrin α11β1 Affects RM11 Prostate and 4T1 Breast Xenograft Tumors Differently. *PLoS ONE,* 11 (3), pp. 1–17.

Rittié L. (2017). Methods for Picrosirius Red-Polarization Detection of Collagen Fibres in Tissue Sections*.* In: L. Rittié (ed) *Fibrosis. Methods in Molecular Biology*, *vol. 1627,* New York, NY: Humana Press Inc*.* pp. 395-407.

Rivenbark, A. G, Connor, S. M. O. and Coleman, W. B. (2013). Molecular and Cellular Heterogeneity in Breast Cancer Challenges for Personalized Medicine. *The American Journal of Pathology,* 183 (4), pp. 1113–1124.

Roussidis, A. E., Mitropoulou, T. N., Theocharis, A. D., Kiamouris, C., Papadopoulos, S., Kletsas, D. and Karamanos, N. K. (2004). STI571 as a Potent Inhibitor of Growth and Invasiveness of Human Epithelial Breast Cancer Cells. *Anticancer Research,* 24 (3), pp. 1445–1447.

Roussidis, A. E., Theocharis, A. D., Tzanakakis G. N. and Karamanos, N. K. (2007). The importance of c-Kit and PDGF receptors as potential targets for molecular therapy in breast cancer. *Current Medical Chemistry,* 14 (7), pp. 735-743.

Raab-Westphal, S., Marshall, J. F. and Goodman, S. L. (2017). Integrins as Therapeutic Targets: Successes and Cancers. *Cancers,* 9 (110), pp. 1–28.

Samoszuk, M. and Corwin, M. A. (2003). Acceleration of Tumor Growth and Peri-Tumoral Blood Clotting by Imatinib Mesylate (Gleevec). *International Journal of Cancer,* 106 (5), pp. 647–652.

Savage, D. G. and Antman, K. H. (2002). Imatinib Mesylate - a New Oral Targeted Therapy. *New England Journal of Medicine,* 346 (9), pp. 683–693.

Sawdon, M. and Kirkman, E. (2017). Capillary Dynamics and the Interstitial Fluid–lymphatic System. *Anaesthesia and Intensive Care Medicine,* 18 (6), pp. 309–315.

Sawyer, D. C. (2008). The Anesthetic Period. In *The Practice of Veterinary Anesthesia: Small Animals, Birds, Fish and Reptiles*. Jackson, WY: Teton Media, pp. 156-164.

Scallan, J., Korthuis, R. and Huxley, V. (2010). Fluid Movement Across the Endothelial Barrier. In D. N. Gragner and J. Granger (eds) *Cappilary Fluid Exchange*. 2nd ed. San Rafael, CA: Morgan and Claypool, pp. 1-21

Schito, L. and Rey, S. (2017). Hypoxic Pathobiology of Breast Cancer Metastasis. *BBA - Reviews on Cancer,* 1868 (1), pp. 239–45.

Schnittert, J., Bansal, R., Storm, R. and Prakash, J. (2018). Integrins in Wound Healing, Fibrosis and Tumor Stroma: High Potential Targets for Therapeutics and Drug Delivery. *Advanced Drug Delivery Reviews,* 129, pp. 37–53.

Srichai, M. B. and Zent, R. (2010). Integrin Structure and Function. In R. Zent and A. Pozzi (eds) *Cell-Extracellular Matrix Interactions in Cancer*. New York, NY: Springer-Verlag, pp. 19-36.

Sener, E., Sipal, S. and Gundogdu, C. (2016). Comparison of Microvessel Density with Prognostic Factors in Invasive Ductal Carcinomas of the Breast. *Turkish Journal of Pathology,* 32 (3), pp. 164–170.

Senger, D. R. and Davis, G.E. (2011). Angiogenesis. *Cold Spring Harbor Perspectives in Biology,* 3, pp. 1–19.

Shah, D., Naciri, M., Clee, P. and Al-Rubeai, M. (2006). NucleoCounter — An Efficient Technique for the Determination of Cell Number and Viability in Animal Cell Culture Processes. *Cytotechnology,* 51, pp. 39–44.

Shaoxian, T., Baohua, Y., Xiaoli, X., Yufan, C., Xiaoyu, T., Hongfen, L., Rui, B., Xiangjie, S., Ruohong, S. and Wentao, Y. (2017). Characterisation of GATA3 Expression in Invasive Breast Cancer: Differences in Histological Subtypes and Immunohistochemically Defined Molecular Subtypes. *Journal of Clinical Pathology,* 70 (11), pp. 926-934.

Shattil, S. J., Kim, C. and Ginsberg, M. H. (2010). The Final Steps of Integrin Activation: The End Game. *Nature Reviews Molecular Cell Biology,* 11 (4), pp. 288–300.

Sortland, K. (2014). *The effect of integrin β3-deficiency on 4T1 mammary tumors in mice.* Msc. University of Bergen.

Sotiriou, C., Neo, S-Y., McShane, L. M., Korn, E. L., Long, P. M., Jazaeri, A., Martiat, P., Fox, S. B., Harris, A. L. and Liu, E. T. (2003). Breast Cancer Classification and Prognosis Based on Gene Expression Profiles from a Population-Based Study. *Proceedings of the National Academy of Sciences of the United States of America,* 100 (18), pp. 10393–10398.

Starling, E. H. (1896). On the Absorption of Fluids from the Connective Tissue Spaces. *The Journal of Physiology,* 19 (4), pp. 312–326.

Stylianopoulos, T., Munn, L. L. and Jain, R. K. (2018). Reengineering the Physical Microenvironment of Tumors to Improve Drug Delivery and Efficacy: From Mathematical Modeling to Bench to Bedside. *TRENDS in CANCER,* 4 (4), pp. 292–319.

Sugiura, K. and Stock, C. C. (1952). Studies in a Tumor Spectrum. *Cancer,* 5 (2), pp. 382–402.

Sun, Z., Guo, S. S. and Fässler, R. (2016). Integrin-Mediated Mechanotransduction. *Journal of Cell Biology,* 215 (4), pp. 1–12.

Svendsen, S., Barczyk, M., Popova, S. N., Lidén, A., Gullberg, D. and Wiig, H. (2009). The α11β1 Integrin Has a Mechanistic Role in Control of Interstitial Fluid Pressure and Edema Formation in Inflammation. *Arteriosclerosis, Thrombosis, and Vascular Biology,* 29 (11), pp. 1864–1870.

Sørlie, T., Perou, C. M., Tibshirani, R., Aas, T., Geisler, S., Johnsen, H., Hastie, T., Eisen, M. B., van der Rijn, M., Jeffrey, S. S., Thorsen, T., Quist, H., Matese, J. C., Brown, P. O., Botstein, D., Lønning, P. E. and Børresen-Dale, A-L. (2001). Gene Expression Patterns of Breast Carcinomas Distinguish Tumor Subclasses with Clinical Implications. *Proceedings of the National Academy of Sciences of the United States of America,* 98 (19), pp. 10869–10874.

Sørlie, T. (2004). Molecular Portraits of Breast Cancer: Tumour Subtypes as Distinct Disease Entities. *European Journal of Cancer,* 40 (18), pp. 2667–2675.

Theocharis, A. D., Skandalis, S. S., Gialeli, C. and Karamanos, N. K. (2016). Extracellular Matrix Structure. *Advanced Drug Delivery Reviews,* 97, pp. 4–27.

ThermoFischer.com. (2018). Overview of Immunohistochemistry (IHC). [online] https://www.thermofisher.com/no/en/home/life-science/protein-biology/protein-biology-learning-center/protein-biology-resource-library/pierce-protein-methods/overview-immunohistochemistry.html [Accessed 19. July 2018].

Uzzan, B., Nicolas, P., Cucherat, M. and Perret, G-Y. (2004). Microvessel Density as a Prognostic Factor in Women with Breast Cancer: A Systematic Review of the Literature and Meta-Analysis. *Cancer Research,* 64, pp. 2941–2955.

VanGundy, Z. C., Markowitz, J., Baker, J. D., Strange, H. R. and Papenfuss, T. L. (2014). An In Vitro Model System to Generate Breast Cancer MDSCs and Study Immune Cell Interactions in Immunocompetent C57bl/6 Mice. *Journal of Cancer Biology and Research,* 2 (1), pp. 1–5.

van´t Veer, Laura J., Hongyue Dai, Marc J. van de Vijver, Yudong D. He, Augustinus A. M. Hart, Mao Mao, Hans L. Peterse, H. L., va der Kooy, K., Marton, M. J., Witteveen, A. T., Schreiber, G. J., Kerkhoven, R. M., Roberts, C., Linsley, P. S., Bernards, R. and Friend, S. H. (2002). Gene Expression Profiling Predicts Clinical Outcome of Breast Cancer. *Nature,* 415 (6871), pp. 530–536.

Velling, T., Kusche-Gullberg, M., Sejersen, T. and Gullberg, D. (1999). cDNA Cloning and Chromosomal Localization of Human α11 Integrin. *The Journal of Biological Chemistry,* 274 (36), pp. 25735–25742.

Vici, P., Pizzuti, L., Natoli, C., Gamucci, T., Di Lauro, L., Barba, M., Sergi, D., Botti, C., Michelotti, A., Moscetti, L., Mariani, L., Izzo, F., D´Onofrio, L., Sperdutti, I., Conti, F., Rossi, V., Cassano, A., Maugeri-Sacca, M., Mottolese, M. and Marchetti, P. (2015). Triple Positive Breast Cancer: A Distinct Subtype? *Cancer Treatment Reviews,* 41 (2), pp. 69–76.

Vlahovic, G., Ponce, A. M., Rabbani, Z., Salahuddin, F. K., Zgonjanin, L., Spasojevic, I., Vujaskovic, Z. and Dewhirst, M. W. (2007). Treatment with Imatinib Improves Drug Delivery and Efficacy in NSCLC Xenografts. *British Journal of Cancer,* 97 (6), pp. 735–740.

Vlahovic, G, Rabbani, Z., Herndon II, J. E., Dewhirst, M. W. and Vujaskovic, Z. (2006). Treatment with Imatinib in NSCLC is Associated with Decrease of Phosphorylated PDGFR-B and VEGF Expression, Decrease in Interstitial Fluid Pressure and Improvement of Oxygenation. *British Journal of Cancer,* 95, pp. 1013–1019.

Vogel, B., Siebert, H., Hofmann, U. and Frantz, S. (2015). Determination of Collagen Content within Picrosirius Red Stained Paraffin-Embedded Tissue Sections Using Fluorescence Microscopy. *MethodsX,* 2, pp. 124–134.

Vogelstein, B. and Kinzler, K. W. (2015). The Path to Cancer - Three Strikes and You´re out. *New England Journal of Medicine,* 373 (20), pp. 1893–1895.

Vogelstein, B., Papadopoulos, N., Velculescu, V. E., Zhou, S., Diaz, L. A. and Kinzler, K. W. (2013). Cancer Genome Landscapes. *Science,* 339 (6127), pp. 1546–1558.

Vogelstein, B. and Kinzler, K. W. (2004). Cancer Genes and the Pathways They Control. *Nature Medicine,* 10 (8), pp. 789–799.

Vong, S. and Kalluri, R. (2011). The Role of Stromal Myofibroblast and Extracellular Matrix in Tumor Angiogenesis. *Genes & Cancer,* 2 (12), pp. 1139–1145.

Wagner, M. and Wiig, H. (2015). Tumor Interstitial Fluid Formation, Characterization, and Clinical Implications. *Frontiers in Oncology,* 5 (115), pp. 1–12.

Wang, J. H. C., Thampatty, B. P., Lin, J. S. and Im, H. J. (2007). Mechanoregulation of Gene Expression in Fibroblasts. *Gene,* 391 (1–2), pp. 1–15.

Wang, Y., Klijn, J. G. M., Zhang, Y., Sieuwerts, A. M., Look, M. P., Yang, F., Talantov, D., Timmermans, M., Meijer-van Gelder, M. E., Yu, J., Jatkoe, T., Berns, E. M., Atkins, D. and Foekens, J. A. (2005). Gene-Expression Profiles to Predict Distant Metastasis of Lymph-Node-Negative Primary Breast Cancer. *Lancet,* 365 (9460), pp. 671–679.

Weidner, N., Semple, J. P., Welch, W. R. and Folkman, J. (1991). Tumor Angiogenesis and Metastasis - Correlation in Invasive Breast Carcinoma. *New England Journal of Medicine,* 324 (1), pp. 1–8.

Weigel, M. T., Meinhold-Heerlein, I., Bauerschlag, D. O., Schem, C., Bauer, M., Jonat, W., Maass, N. and Mundhenke, C. (2009). Combination of imatinib and vinorelbine enhances cell growth inhibition in breast cancer cells via PDGF beta signalling. *Cancer Letters,* 273 (1), pp. 70-79.

Whittle, J. R., Lewis, M. T., Lindeman, G. J. and Visvader, J. E. (2015). Patient-Derived Xenograft Models of Breast Cancer and Their Predictive Power. *Breast Cancer Research,* 17 (17), pp. 1-13.

Wiig, H. and Swartz, M. A. (2012). Interstitial Fluid and Lymph Formation and Transport: Physiological Regulation and Roles in Inflammation and Cancer. *Physiological Reviews,* 92 (3), pp. 1005–1060.

Wiig, H., Reed, R. K. and Aukland, K. (1986). Measurement of Interstitial Fluid Pressure: Comparison of Methods. *Annals of Biomedical Engineering,* 14 (2), pp. 139–151.

Yang, Y., Sun, M., Wang, L. and Jiao, B. (2013). HIFs, Angiogenesis, and Cancer. *Journal of Cellular Biochemistry,* 114 (5), pp. 967–974.

Yersal, O. and Barutca, S. (2014). Biological Subtypes of Breast Cancer: Prognostic and Therapeutic Implications. *World Journal of Clinical Oncology,* 5 (3), pp. 412–424.

Zeltz, C. and Gullberg, D. (2016). The Integrin-Collagen Connection - a Glue for Tissue Repair? *Journal of Cell Science,* 129 (4), pp. 1–12.

Östman, A. (2017). PDGF Receptors in Tumor Stroma: Biological Effects and Associations with Prognosis and Response to Treatment. *Advanced Drug Delivery Reviews,* 121, pp. 117–123.

8 Appendix A

Genotyping of integrin α11-deficient mice

Solutions:

MGB stock solution:
8400 µL MilliQ
1000 µL 10x MGB
100 µL Mercaptoethanol
500 µL Triton X-100 (diluted 1:10 in MilliQ)

Proteinase K (2 mg/mL):
Dilute proteinase K in RNase free water (2 mg/mL)

PCR stock solution:
Mix stock solution in an Eppendorf tube. Use RNase free pipets and work on ice.

Solutions	**1x**	**27x**
10 x buffer-$MgCl_2$	2 µl	54 µl
dNTP 10 mM	0,4 µl	10,8 µl
Ko-wt fw and rew	0,5+0,5 µl	13,5+13,5 µl
Lac z1 and lac z2	0,25+0,25 µl	6,75+6,75 µl
Polymerase (5u/ml)	0,1 µl	2,7 µl
H20	14 µl	378 µl
DNA	2µl µl	2 µl
Totalt	**20 µl**	

Purification:
-Add 40 µL MGB stock to each earpiece and heat inactivate at 95^{0}C for 5 min, using a heat block shaker.
-Cool PCR tubes on ice and add 2 µl proteinase K to each tube, and incubate at 56^{0}C for 1 hour, using a heat block shaker.
-Heat inactivate at 95^{0}C for 5 min, using a heat block shaker.
-Centrifuge for 10 min.
-Dilute the samples 1:5 in buffer

PCR:
Mix PCR stock solution and distribute 18 µl to each PCR tube. Add 2 µl purified DNA.
Run PCR program GT-KOWT.

Separation:

-Dissolve 1 g agarose in 50 µl TAE buffer (1 gel), boil in microwave until completely dissolved.
-Add 3 µl GelRed TM Nucleic acid gel stain and swirl the flask until completely dissolved.
-Pour gel in rack at leave it for 20-30 min.
-Add buffer to separation rack.

-Add 4 µl loading dye to each sample.
-Load 10 µl sample in wells.
-Load 5 µl ladder
-run gel at 90 V for 20-30 min
- Develop image